scientific reports

OPEN

Electrochemical, surface morphological and computational evaluation on carbohydrazide Schiff bases as corrosion inhibitor for mild steel in acidic medium

Sujata Kumari Gupta[1], R. K. Mitra[1], Mahendra Yadav[1✉], Omar Dagdag[2,3], Avni Berisha[4], Bhekie B. Mamba[3], Thabo T. I. Nkambule[3], Eno E. Ebenso[2,3✉] & Shailendra Kumar Singh[5]

Anticorrosion and adsorption behaviour of synthesized carbohydrazide Schiff bases, namely (Z)-*N'*-(4-hydroxy-3-methoxybenzylidene)-6-methyl-2-oxo-4-phenyl-1,2,3,4-tetrahydropyrimidine-5-carbohydrazide(MBTC) and (Z)-*N'*-(3,4-dichlorobenzylidene)-6-methyl-2-oxo-4-phenyl-1,2,3,4-tetrahydropyrimidine-5-carbohydrazide (CBTC) was examined for mild steel (MS) in 15% HCl medium. The corrosion inhibition study was performed by using gravimetric, thermodynamic, electrochemical and theoretical studies including density functional theory (DFT), molecular dynamic simulation (MDS) and Monte Carlo simulations (MCS). The outcomes in terms of corrosion inhibition efficiency using electrochemical impedance spectroscopy (EIS) method at 303 K and 150 ppm concentration were 96.75% for MBTC and 95.14% for CBTC. Both inhibitors adsorbed on the MS surface through physical as well as chemical adsorption and followed the Langmuir isotherm. The mixed-type nature of both inhibitors was identified by polarization results. Surface analysis was done using FESEM, EDX, AFM and XPS studies and results showed that a protective layer of inhibitor molecules was developed over the surface of MS. The results of DFT, MCS and MDS are in accordance with experimental results obtained by weight loss and electrochemical methods.

The research on corrosion inhibition is considered as a challenging problem because corrosion is spontaneous and continuous degradation of metallic structures using electrochemical and chemical reactions with the surrounding, which cause severe safety and economic loss in various sectors[1]. The mild steel (MS) is considered as core structural element in many industries due to its effective potency in flexibility and cheaper cost. Many industries use solution of HCl and H_2SO_4 for acid pickling of steel and iron, production of ore, oil well acidization and removal of rust as well as scale. During these operations, due to the corrosive properties of acid solution, severe corrosion of metal happens which creates environmental as well as economic issues[2,3]. To minimize this loss, various corrosion prevention techniques like coating, selection of alloy, galvanization, cathodic and anodic protections, and selection of inhibitors are used. From these methods, addition of corrosion inhibitors in the solution phase is the most useful techniques for prevention of corrosion[4]. The adsorption of corrosion inhibitors on MS surface depends on the structure of corrosion inhibitor and played a significant role in the formation of corrosion protecting film on the surface of MS. The addition of small amount of the corrosion inhibitor provides rise in efficiency by instantly decreasing the corrosion rate[5]. In application of corrosion inhibitors, industries are facing challenge because most of the corrosion inhibitor molecules are toxic and harmful for both human and environment. The compounds containing functional groups such as NH_2, OH, OCH_3, C=N, C=O, SH, and hetero atoms like O, N, P, S as well as unsaturated aromatic system work as efficient inhibitors[6–12]. Schiff bases

[1]Department of Chemistry and Chemical Biology, Indian Institute of Technology (ISM), Dhanbad, Jharkhand 826004, India. [2]Centre for Materials Science, College of Science, Engineering and Technology, University of South Africa, Johannesburg 1710, South Africa. [3]Institute of Nanotechnology and Water Sustainability, College of Science, Engineering and Technology, University of South Africa, Johannesburg 1710, South Africa. [4]Department of Chemistry, Faculty of Natural and Mathematics Science, University of Prishtina, 10000 Prishtina, Kosovo. [5]Department of Chemistry, Hansraj College, University of Delhi, Delhi 110007, India. ✉email: mahendra@iitism.ac.in; ebensee@unisa.ac.za

showed excellent inhibition efficiency for different metals and alloys such as copper, brass, aluminum, MS, and stainless steel in different corrosive mediums. Presently Schiff bases are used as inhibitor because of their simple synthetic procedure, low-cost, high-yield and less toxic properties. Apart from these, Schiff base compounds are also used in catalysis, photochromic field, and medicine[13]. Because of easy synthesis, high efficiency and low toxicity, Schiff base compounds are good choice in selection of inhibitors and various researchers have used Schiff base compounds as corrosion inhibitor[14,15]. The Schiff base compound reported as corrosion inhibitor in literature for MS in HCl medium[16–30] are represented in Table 1.

Inspired with the use of Schiff base compounds as efficient and low toxic corrosion inhibitors and with expectation of higher inhibition efficiency as compared to reported inhibitors, in the present investigation carbohydrazide Schiff base compounds, (Z)-N'-(3,4-dichlorobenzylidene)-6-methyl-2-oxo-4-phenyl-1,2,3,4-tetrahydropyrimidine-5-carbohydrazide(CBTC)and (Z)-N'-(4-hydroxy-3-methoxybenzylidene)-6-methyl-2-oxo-4-phenyl-1,2,3,4-tetrahydropyrimidine-5-carbohydrazideon (MBTC) were prepared for corrosion inhibition study of MS in 15% HCl. The selection of Schiff bases was done according to their planar structure and good molecular framework which promotes better inhibition efficiency. Two Schiff bases were taken with the same moiety, but different substitution groups to study the effect of substituent's on corrosion inhibition behavior of the inhibitors.

Experimental procedure

Synthesis of carbohydrazide Schiff base inhibitors.
Both the inhibitors were prepared in the laboratory as per reported procedure[31] as shown in Fig. 1. The mixture of urea (0.15 mol), ethyl acetoacetate (0.1 mol), benzaldehyde, ethanol (25–30 mL) and conc. HCl in 3-drops was refluxed for 1:30 h. After completion of the reaction, reaction mixture was put into ice cold water with continuous stirring, then it was kept for 18 h, mixture was filtered and dried. The compound formed was called *biginelli*, it was recrystallized through ethanol and tested by thin layer chromatography. After recrystallization, mixture of *biginelli* (0.01 mol), hydrazine hydrate, ethanol (approx. 20–22 mL) and 4-drops of conc. H_2SO_4 was refluxed for 3 h. After completion of reaction, the mixture was recrystallized through ethanol and the product formed was called carbohyrazido compound. The mixture of carbohyrazido (0.01 mol), substituted aromatic aldehyde, ethanol (20 mL) and 5 mL of glacial acetic acid was refluxed for 2 h. Upon the accomplishment of reaction, it was placed into cold water, the product was filtered and dried. TLC was used to test the purity of the compound, the precipitate was recrystallized using ethanol and the obtained compounds are MBTC and CBTC. Both compounds were characterized and obtained data are as follows:

MBTC. Mol. Formulae: $C_{20}H_{20}N_4O_4$, Mol. Weight: 380.40, Yield: 78%, Elemental analysis: calculated %weight- C: 63.15, N: 14.73, H: 5.30, O: 16.82.
FTIR, (cm^{-1}) 3551.75(NH), 3484.26(OH), 3244.16(NH in amide), 3124.6 (AR–CH), 2931.75 (Aliphatic CH), 1700.91(C=O in amide), 1648.36 (C=O), 1091.99 (C–O–C).

CBTC. Mol. Formulae: $C_{19}H_{16}Cl_2N_4O_2$, Mol. Weight: 403.26, Yield: 80%, Elemental analysis: calculated %weight- C: 56.59, N: 13.89, O: 7.93, Cl: 17.58, H: 4.00.

S. no	Inhibitor	Medium	Material	Inhibition efficiency (η %)	Conc. (ppm)	Ref
1	Potassium-(2-(((1H-indol-3-yl)methylene)amino)acetyl) tyrosinate [GTI]	1 M HCl	Mild Steel	98.70	403	16
2	N,N'-(1,3-phenylene)bis(1-(pyridin-2-yl)methanimine) [PBPM]	1.0 mol^{-1} HCl	Mild Steel	78.35	800	17
3	4-((2,3-dichlorobenzylidene) amino) -3-methyl-1H-1,2,4-triazole-5(4H)-thione, [CBAT]	1 M HCl	Mild Steel	95.00	287	18
4	N,N'-(1,4-phenylene)bis(1-(pyridin-3-yl)methan-imine) [PBPM3]	1 M HCl	Mild Steel	83.92	800	19
5	(1E,2E)-N-(3-(1H-imidazol-1-yl)propyl)-3-phenylprop-2-en-1-imine [ICSB]	1 M HCl	Mild Steel	98.80	239	20
6	2-((E)-((E)-2-hydrazone-1,2-diphenylethylidene)amino phenol) [HDAP]	1 M HCl	Mild Steel	92.76	3153	21
7	4,4'-Oxybis N-[(E)quinoleine-2-ylmethylidene]aniline[OQ]	1 M HCl	Mild Steel	86.46	2392	22
8	Vanillin cyanoguanidine imine [VCNG]	1 M HCl	Mild Steel	93.10	499	23
9	2-(2-oxoindolin-3-ylidene) hydrazinecarbothioamide [OHB]	1 M HCl	Mild Steel	96.00	220	24
10	(E)-4-(1-(pyridin-2 ylimino) ethyl)benzene-1,3-diol [PSB2]	1 M HCl	Mild Steel	90.00	228	25
11	3,3'-dimethoxy-5,5'-bis((E)-((pyridin2ylmethyl)imino)methyl)-[1,1'-biphenyl]-2,2'-diol [vanillin based]	1 M HCl	Mild Steel	95.30	482	26
12	4,4'-bis(2-furylideneimino)biphenyl]-4,4'-diamine [HL2)]	1 M HCl	Mild Steel	89.41	340	27
13	N-(2-((Z)-2-(3-methoxy-4-hydroxybenzylideneamino) ethylamino)ethyl)-3,4,5-trihydroxybenzamide [VA]	0.5 M HCl	Mild Steel	88.52	250	28
14	N-[(Z)-1-phenylemethyleidene]-N-{2-[2-{[[(Z)-1-phenylmethylidene]amino}phenyl] disulfanyl]phenyl}amine	2.0 M HCl	Mild Steel	96.00	424	29
15	(1,2-1H-Benzoimidazol-2-yl)-(1,2-diphenyl-ethylidene)-amine [BDEA]	1.0 M HCl	Mild Steel	96.85	400	30

Table 1. Summary of already reported Schiff bases as corrosion inhibitors for MS in HCl solution.
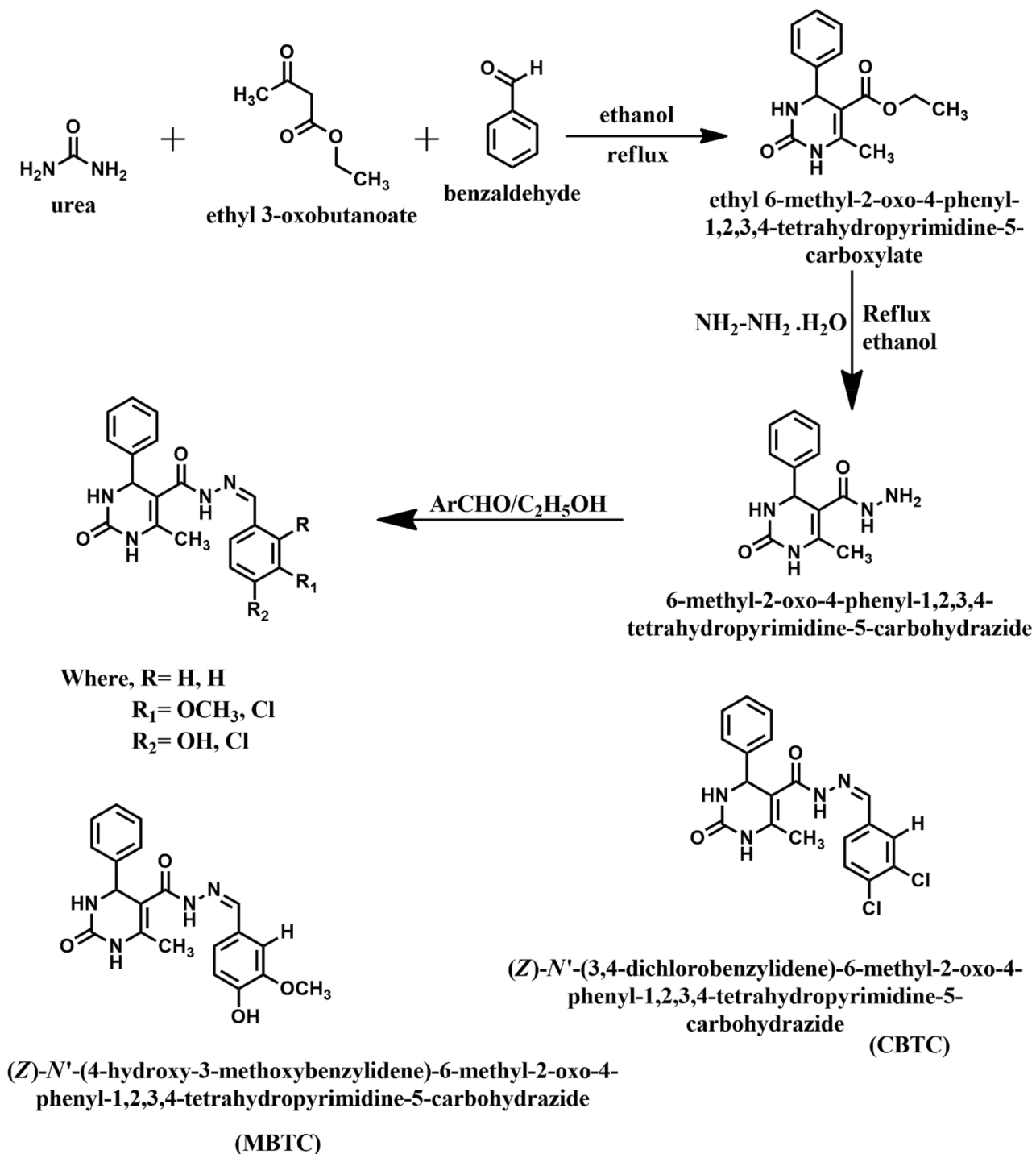
Figure 1. Reaction scheme of MBTC and CBTC synthesis.

FTIR (cm^{-1}) 3421.58(NH), 3244.16 (NH in amide), 3114.47 (Ar–CH), 2937.06 (Aliphatic CH), 1700.91 (C=O in amide), 781.99 (C–Cl).

Material. All investigations were conducted using MS with elemental percentage composition, as; Sn: 0.03, Ni: 0.02, Mn: 0.13, Cu: 0.01, P: 0.02, C: 0.13 along with Fe (iron: rest elemental percentage). MS was cut into the dimension of 3.5 cm×3.0 cm×0.1 cm for gravimetric method and for electrochemical analysis 1.0 cm×1.0 cm×0.1 cm individually. Several grades (i.e., 80 to 2000) of emery paper were used to clean the MS surface before each experiment successively so that homogeneous surface was obtained. These samples were then thoroughly cleaned in an ultrasonic cleaner for 15 min, cleaned with acetone, and dried. The solution of inhibitor concentrations ranging from 0 to 150 ppm was made in 15% HCl by dilution of analytical grade 37% HCl with distilled water.

Gravimetric Analysis. Gravimetric analysis was used to investigate how temperature and concentration affected the examined Schiff base ability to prevent corrosion. MS specimens were submerged in 500 mL 15% HCl solution for 6 h at different temperatures ranging from 303 to 333 K, without and with several concentration of synthesized carbohydrazide Schiff base inhibitors. The specimens were weighed before and after submersion and weight loss was calculated. Each experimental value was calculated from the average data of triplicate value of weight loss[32]. The corrosion rate (CR), efficiency (η%) and surface coverage (θ) were calculated as follows:

$$CR(mmyear)^{-1} = \frac{W * 8.76 * 10^4}{T * D * A} \tag{1}$$

where average weight loss is represented by W, sample area by A, immersion time by T (in hours), and sample density by D (in gm cm^{-3}). The efficiency (η %) along with surface coverage (θ) of the investigated inhibitor are calculated by utilizing the Eqs. (2) and (3), as below:

$$\eta\% = \frac{CR_0 - CR_I}{CR_0} * 100 \tag{2}$$

$$\theta = \frac{\eta\%}{100} \tag{3}$$

where CR_0 and CR_I, stands for corrosion rates without and with synthesized carbohydrazide Schiff base inhibitors.

Electrochemical analysis. Electrochemical analysis was executed in conventional 3-electrode system cell by the electrochemical corrosion analyzer (CS-350) monitoring through CS Studio. Saturated calomel electrode act as the reference electrode, platinum electrode serves as the counter electrode and MS with surface area of 1cm^2 serve as working electrode. Before starting the experiment, the cells' working electrode is maintained in contact with 200 mL of acidic solution for 1800s for attaining steady state condition. Later potentials were examined in the range of ±2.5V with a scan rate of at 0.5 mV s^{-1} from OCP which provides the polarization curves. Subsequently, at an open circuit voltage and frequency range of 100 kHz to 1Hz, electrochemical impedance spectroscopy (EIS) was evaluated[33].

Surface analysis. For surface analysis the MS specimen was prepared by pervious procedure as described from weight loss analysis. Before and after adding 150 ppm of inhibitor at 303 K, the MS surface was submerged for 6 h in 15% HCl medium. The specimen was removed after 6 h and washed with distilled water and then dried and further sampled for FESEM, EDX, AFM and XPS analysis[34].

Computational studies. *Quantum chemical calculations.* All quantum chemistry calculations have been implemented with full geometric optimizations utilizing the Dmol3 module integrated into the Biovia Materials studio software. The geometric structures of the studied molecules were attained through global optimizations characterized by a calculation of the vibration frequencies using the DFT method by utilizing Dmol3, including the B3LYP/DND/COSMO (water) model[34–40].

MC and MD simulations. Materials Studio 8.0, programmed created by Accelrys Inc, was used to run MC and MD[41–44]. A three-dimensional geometry simulation box whose dimensions are (24.823752 × 24.823752 × 18.241 658) was used for simulations of the interaction between the MBTC along with CBTC molecules and the surface of Fe (110). The MDS were worked at a temperature of 298 K and the motion equations were integrated under the NVT canonical ensemble utilizing the COMPASS force field, with a time step of 1 fs and a simulation time of 800 ps. This model included Fe layer, 15 hydronium, 15 chloride, 700 H$_2$O molecules and 1 inhibitor molecule and a 35 vacuum layer were involved in the simulation box.

Results and discussion
Gravimetric analysis. The gravimetric analysis is a first step in the investigation of corrosion inhibition. The effect of concentration on the inhibition efficiency (η %) and corrosion rate (CR) for the MS in 15% HCl at various temperatures (303 K–333 K) was done and obtained corrosion parameters are specified in Table 2. According to Table 2 and Fig. 2, it is found that, as the surface coverage of MS grew, the CR gradually dropped and corrosion inhibition (η %) gradually increased with rising inhibitor concentration. This indicated that sample surface is protected through the molecule of inhibitors during the increase in concentration as they are absorbed on the MS surface. Thus, the highest inhibitory efficiency obtained was at 150 ppm of MBTC as 96.78%, and it was 95.09% for CBTC. The higher efficiency of MBTC is because of the presence of electron donor group –OCH$_3$, imine, carbonyl groups and heterocyclic rings (Fig. 1) which improved the efficiency level in the transfers of unpaired electrons from inhibitor molecules to the vacant d-orbital of Fe, which develops a coordinate-bond and thus slows the rate of corrosion (CR)[45]. The decrease in the inhibition potency on increase in temperature was observed due to removal of adsorbed inhibitory layer from MS surface. As per literature review, corrosion inhibition studies of MBTC and CBTC is not reported and both inhibitors offered better efficiency than most of the similar type of inhibitors reported in literature[16–30] as shown in Table 1. Therefore the work reported in the present investigation is novel and has potential industrial application.

	303 K			313 K			323 K			333 K		
	(CR)	(θ)	η %	(CR)	(θ)	η %	(CR)	(θ)	η %	(CR)	(θ)	η %
Conc	mm y^{-1}			mmy^{-1}			mmy^{-1}			mmy^{-1}		
0	20.60	–	–	49.64	–	–	70.24	–	–	106.87	–	–
MBTC												
15	4.492 ± 0.016	0.781	78.19 ± 0.080	14.20 ± 0.166	0.713	71.38 ± 0.336	23.11 ± 0.154	0.673	67.32 ± 0.220	38.95 ± 0.093	0.635	63.55 ± 0.087
30	3.409 ± 0.056	0.834	83.45 ± 0.027	11.17 ± 0.057	0.774	77.48 ± 0.115	18.95 ± 0.017	0.732	73.20 ± 0.172	34.09 ± 0.364	0.681	68.10 ± 0.341
50	2.474 ± 0.118	0.879	87.99 ± 0.057	8.165 ± 0.105	0.835	83.55 ± 0.212	14.93 ± 0.017	0.788	78,89 ± 0.406	28.73 ± 0.234	0.731	73.11 ± 0.219
75	1.555 ± 0.038	0.924	92.45 ± 0.018	5.385 ± 0.084	0.891	89.15 ± 0.170	12.62 ± 0.021	0.821	82.15 ± 0.266	23.94 ± 0.431	0.775	77.59 ± 0.404
100	1.052 ± 0.083	0.948	94.89 ± 0.040	3.916 ± 0.067	0.921	92.11 ± 0.135	11.03 ± 0.024	0.844	84.40 ± 0.28	21.21 ± 0.564	0.801	80.15 ± 0.527
150	0.6633 ± 0.030	0.967	96.78 ± 0.014	2.536 ± 0.035	0.948	94.89 ± 0.070	9.196 ± 0.198	0.87	87.00 ± 0.282	17.53 ± 0.119	0.835	83.59 ± 0.111
200	0.5253 ± 0.048	0.974	97.45	2.233 ± 0.020	0.955	95.55 ± 0.413	8.849 ± 0.113	0.879	87.99 ± 0.13	16.15 ± 0.845	0.848	84.88 ± 0.532
CBTC												
15	5.172 ± 0.011	0.748	74.89 ± 0.055	14.79 ± 0.341	0.701	70.19 ± 0.688	24.12 ± 0.302	0.659	65.90 ± 0.430	38.95 ± 0.351	0.635	63.55 ± 0.328
30	4.089 ± 0.047	0.801	80.15 ± 0.229	11.64 ± 0.405	0.765	76.55 ± 0.816	20.01 ± 0.653	0.717	71.70 ± 0.929	33.99 ± 0.312	0.681	68.19 ± 0.292
50	2.931 ± 0.098	0.857	85.77 ± 0.479	8.984 ± 0.221	0.819	81.90 ± 0.446	16.97 ± 0.311	0.760	76.00 ± 0.443	28.74 ± 0.107	0.731	73.10 ± 0.100
75	2.06 ± 0.077	0.90	90.00 ± 0.377	6.949 ± 0.186	0.860	86.00 ± 0.376	13.37 ± 0.100	0.810	81.09 ± 0.142	23.75 ± 0.412	0.777	77.77 ± 0.385
100	1.283 ± 0.052	0.937	93.77 ± 0.256	5.862 ± 0.109	0.881	88.19 ± 0.221	10.77 ± 0.161	0.847	84.77 ± 0.229	22.25 ± 0.293	0.791	79.18 ± 0.274
150	1.011 ± 0.036	0.950	95.09 ± 0.176	4.085 ± 0.505	0.917	91.77 ± 1.017	9.111 ± 0.160	0.871	87.12 ± 0.228	19.42 ± 0.119	0.818	81.82 ± 0.111
200	0.8466 ± 0.030	0.958	95.89 ± 0.146	3.430 ± 0.146	0.930	93.09 ± 0.295	7.852 ± 0.561	0.889	88.90 ± 0.547	18.29 ± 0.835	0.828	82.88 ± 0.527

Table 2. Gravimetric parameters of carbohydrazide Schiff base inhibitor.
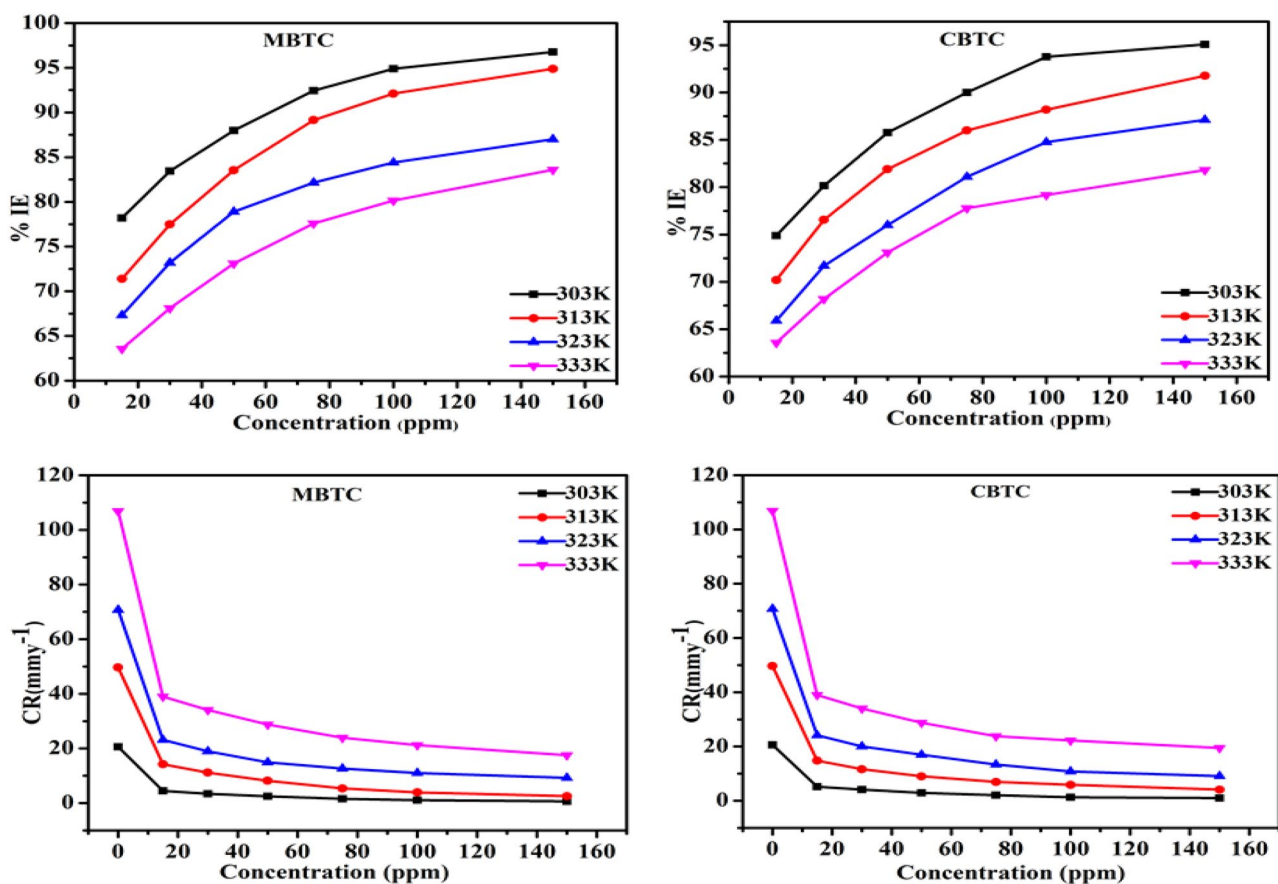

Figure 2. Plot of η % and (CR) at different temperatures for carbohydrazide Schiff base (MBTC and CBTC) inhibitor.

Kinetic and thermodynamic activation parameters. The kinetic and thermodynamic parameters were obtained from Arrhenius and Transition Eqs. 4 and 5 and plots Figs. 3 and 4 as follows:

$$\log(CR) = \frac{-E_a}{2.303RT} + \log A \tag{4}$$

$$CR = \left(\frac{RT}{NH}\right) expo \frac{\Delta S^*}{R} expo \frac{-\Delta H^*}{RT} \tag{5}$$

where activation enthalpy and entropy are represented by ΔH^* and ΔS^* while A is the pre-exponential component called Arrhenius constant respectively. T refers to the absolute temp., and H, N, R, refers to Planck constant, Avogadro number and gas constant respectively. By fitting the Arrhenius and transition plots shown in Figs. 3 and 4 respectively, the values for the activation parameters (E_a) and ΔH^* and ΔS^* were determined and provided in Table 3.

The E_a value of inhibitors MBTC and CBTC for all concentrations are greater than uninhibited value. These demonstrate that a shielding layer was created on the MS surface and makes more resistant to corrosive process. From Table 3, the negative values of ΔS^* reflect that the rate-determining step is the association rather than dissociation of activated complex, and the positive data of ΔS^* denotes an increment in disorder because desorption of more number of water molecules from the surface of MS by adsorption of one molecule of inhibitor while the positive values of ΔH indicate the difficulty in MS dissolution[46].

Adsorption isotherm. Adsorption isotherm studies provide information on the interactions between the inhibitor and the MS surface. The following equation is representation of the Langmuir isotherm,
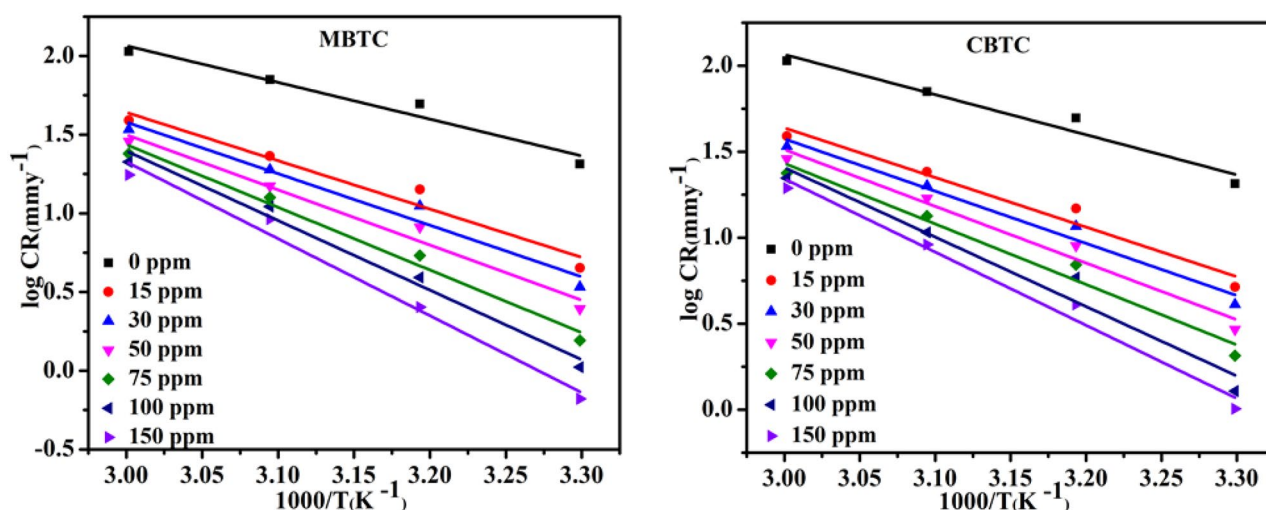

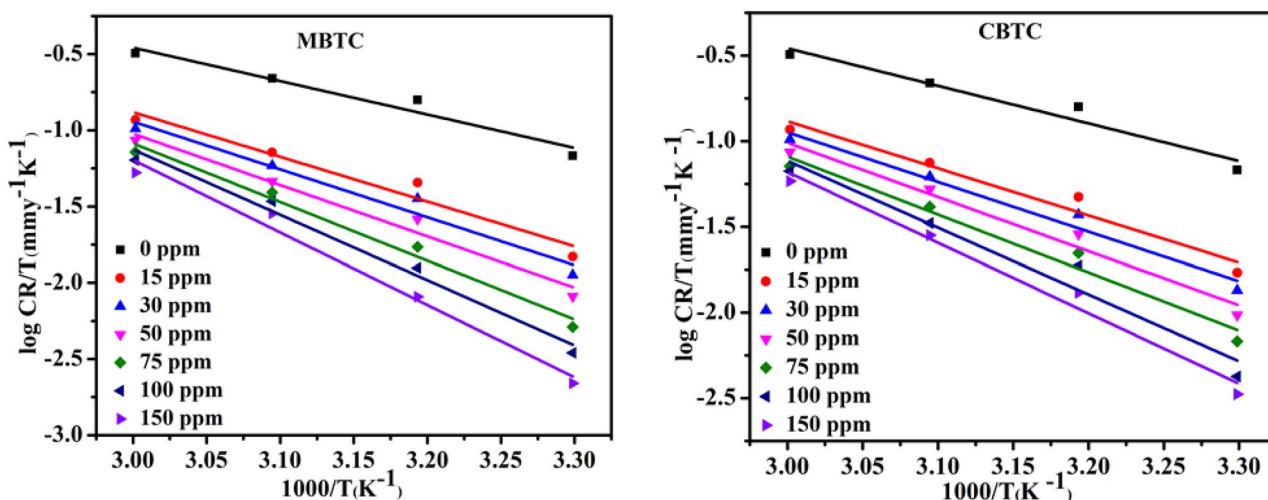**Figure 3.** MBTC and CBTC Arrhenius plot for carbohydrazide Schiff base.

Figure 4. MBTC and CBTC Transition plot for carbohydrazide Schiff base.

Inhibitor	Concentration (ppm)	Ea (kJ mol⁻¹)	ΔH* (kJ mol⁻¹)	ΔS* (Jmol⁻¹ K⁻¹)
Blank	0	44.67	42.02	− 80.23
MBTC	15	58.80	56.15	− 45.94
	30	62.72	60.08	− 35.35
	50	67.09	64.44	− 23.79
	75	76.30	73.65	2.626
	100	84.66	82.02	26.94
	150	93.61	90.96	52.48
CBTC	15	55.23	52.59	− 56.68
	30	58.13	55.48	− 49.22
	50	63.12	60.48	− 35.43
	75	67.37	64.73	− 24.19
	100	77.33	74.69	5.15
	150	81.47	78.82	16.35

Table 3. Thermodynamic and kinetic parameters of carbohydrazide Schiff base inhibitor.

$$\frac{C_{inh}}{\theta} = \frac{1}{K_{ads}} + C_{inh} \tag{6}$$

Different adsorption models were tried with the experimental data, Langmuir isotherm gave a linear plot between $\frac{C_{inh}}{\theta}$ vs Concentrations which are shown in Fig. 5, through which K_{ads} value was calculated. Using K_{ads} value, ΔG^0_{ads} value was derived from the following Eq. 7.

$$\Delta G^0_{ads} = -RTln(55.5K_{ads}) \tag{7}$$

R, T and 55.5 denote the gas constant, absolute temp., and the conc. (mol l⁻¹) for water.

Since the R² as well as slope values for the Langmuir isotherm are very close to one, it has been verified to be a superior fit for the examined value displayed in Table 4.

Experimental data from Table 4, has larger value of K_{ads} indicating superior inhibition efficiency and good interaction between carbohyrazide Schiff base and MS surface whereas lower value of K_{ads} indicates weaker interaction so that adsorbed molecules can be easily removed from MS surface.

The negative ΔG^0_{ads} values suggests that the adsorption of carbohydrazide Schiff base MBTC and CBTC on the surface of MS was proceeding spontaneously and the value of ΔG^0_{ads} obtained for both inhibitors verified physisorption as well as chemisorption adsorption at MS surface. According to the review of literature, ΔG^0_{ads} value less negative than − 20 kJ mol⁻¹ results physisorption whereas more negative than − 40 kJ mol⁻¹ results chemisorptions. Table 4 shows that the values of ΔG^0_{ads} for synthesized carbohydrazide Schiff base in 15% HCl at various temperatures attain the range showing the spontaneous chemisorption and physisorption, which is a mixed nature of adsorption[47].
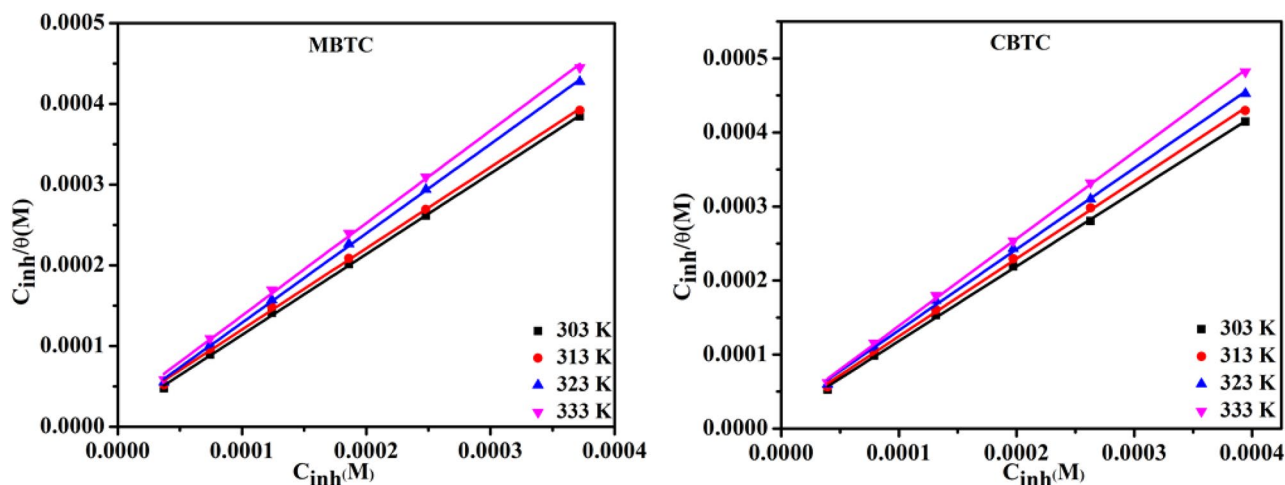

Figure 5. Langmuir plot for MBTC and CBTC inhibitors.

Inhibitors	Temperature K	Slope	K_{ads} M^{-1}	ΔG^0_{ads} kJmol^{-1}	R^2
MBTC	303 K	0.99893	7.14E+04	− 38.27	0.99956
	313 K	1.00586	5.51E+04	− 38.61	0.99955
	323 K	1.10702	5.05E+04	− 40.10	0.99919
	333 K	1.14607	4.35E+04	− 40.69	0.99856
CBTC	303 K	1.00979	5.80E+04	− 37.74	0.99934
	313 K	1.04858	2.80E+04	− 38.63	0.99920
	323 K	1.09589	2.61E+04	− 39.45	0.99935
	333 K	1.17501	2.40E+04	− 40.90	0.99879

Table 4. Adsorption data of carbohydrazide Schiff base inhibitors.
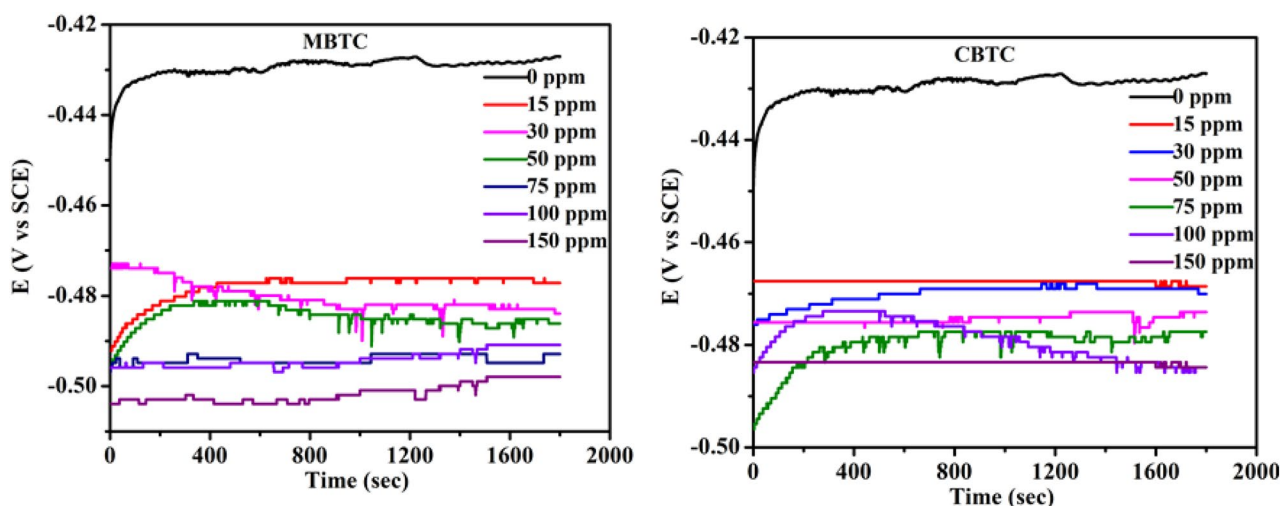
Figure 6. OCP plot for MBTC and CBTC carbohydrazide Schiff base inhibitors.

Electrochemical analysis. *Open circuit potential.* Figure 6 reveals the variation of OCP w.r.t. time in the absence and presence of different dosages of carbohydrazide Schiff base inhibitors at 303 K. Figure 6, displays that the addition of MBTC and CBTC inhibitors shifted the potential to the negative side when compared with pure 15% hydrochloric acid corrosive medium, indicating that both inhibitors are predominantly cathodic. Whereas the obtained data of OCP for the working electrode with various dosages of both inhibitors alter OCP to an extent of less than ± 85 mV vs. OCP data as compared to without inhibitor, indicating that the studied inhibitors are mixed type and dominant towards cathodic nature[48].

Potentiodynamic polarization (PDP). PDP is a significant electrochemical method to know about inhibition efficiency of inhibitor. PDP gives value of corrosion current and corrosion potential of the electrode immersed in corrosive solution. Here. PDP curves were plotted to know the impact of various dosages of carbohydrazide Schiff base inhibitor at MS/15% HCl interface as shown in Fig. 7. PDP variables such as, corrosion potential (E_{corr}), anodic and cathodic slopes (β_a & β_c), and corrosion current density were observed from PDP curves and arranged in Table 5. The efficiency of corrosion prevention was obtained from Eq. (8) below.

$$\%I.E_{(T)} = \frac{i_{corr}^{(inhi)}}{i_{corr}} * 100 \qquad (8)$$

It is noticed that by increase of the conc. of MBTC and CBTC, there is a gradual decrease of i_{corr} value. This observation shows the improvement of a protection film on the MS surface by the adsorption of inhibitor molecules that decreases the dissolution of MS surface. This process is more effective with the increment in the conc. of MBTC and CBTC and reaches maximum at 150 ppm 97.46% and 95.65%, individually. Furthermore, PDP shows very less shift in E_{corr} data (*lessthan* 85 mV) towards more negative side compared to the uninhibited MS, indicating that both inhibitor molecules control anodic as well as cathodic reactions and act as mixed inhibitor. In addition the shift in E_{corr} values and the variation of β_a and β_c values with inhibitor concentration w.r.t. without inhibitor also suggested that studied inhibitors are mixed type inhibitors. From Table 5, the data of β_a and β_c do'nt show regular trend which indicate that both physisorption and chemisorption plays an important role in the corrosion inhibition[49].
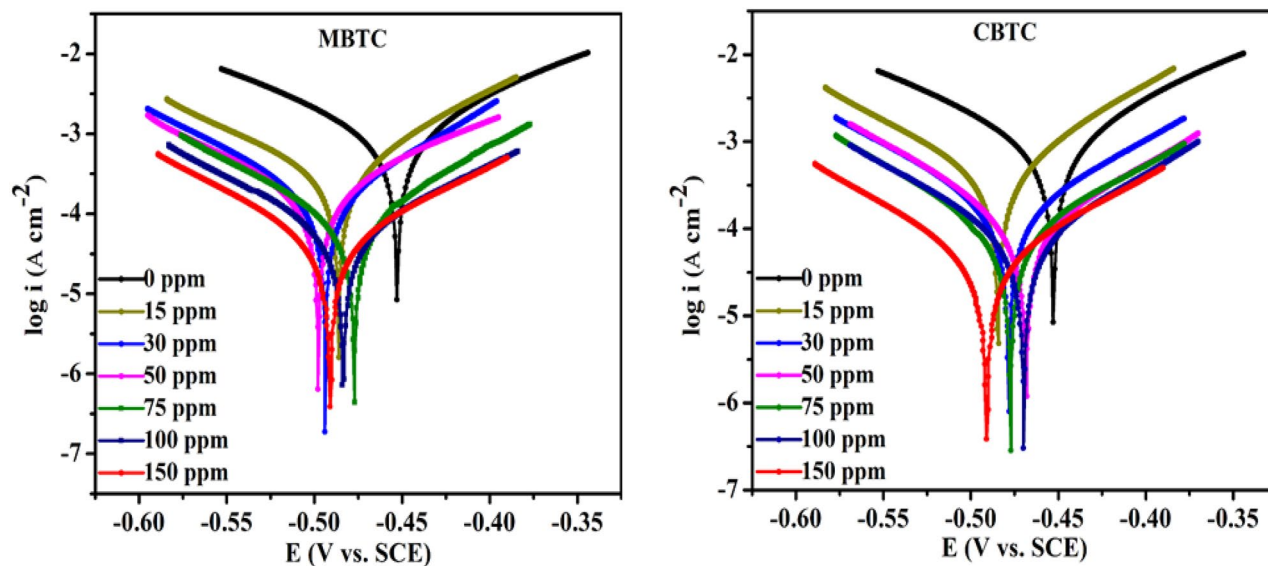
Figure 7. Tafel plot for MBTC and CBTC carbohydrazide Schiff base inhibitors.

Conc. (ppm)	E_{corr} (mV/SCE)	i_{corr} (μA cm⁻²)	β_a (mV dec⁻¹)	$-\beta_c$ (mV dec⁻¹)	IE_T%
0	− 427	2017 (± 0.204)	279	277	–
MBTC					
15	− 477.11	399.08 (± 0.021)	89.97	126.78	80.21 (± 0.0015)
30	− 483.62	234.42 (± 0.301)	119.98	121.60	88.37 (± 0.0002)
50	− 483.92	133.09 (± 0.152)	99.06	91.86	93.40 (± 0.0004)
75	− 486.14	91.46 (± 0.067)	86.06	100.47	95.46 (± 0.0034)
100	− 490.84	69.82 (± 0.038)	108.71	101.12	96.53 (± 0.0047)
150	− 497.83	51.51 (± 0.024)	103.43	96.58	97.46 (± 0.0025)
CBTC					
15	− 468.54	499.48 (± 0.028)	86.88	112.78	75.23 (± 0.0022)
30	− 470.02	354.89 (± 0.019)	102.22	138.17	82.85 (± 0.0007)
50	− 473.58	185.02 (± 0.016)	102.91	97.75	90.82 (± 0.0019)
75	− 477.41	124.25 (± 0.015)	102.69	89.77	93.83 (± 0.0045)
100	− 478.44	102.28 (± 0.030)	104.94	96.20	94.92 (± 0.0006)
150	− 484.38	87.56 (± 0.0132)	97.82	98.30	95.65 (± 0.0075)

Table 5. Polarization data of carbohydrazideschiff base inhibitors.

EIS analysis. EIS is used to correctly measure the inhibition efficiency of an inhibitor. The Nyquist and Bode plots were obtained without and with MBTC and CBTC inhibitors as depicted in Figs. 8 and 9, respectively. Nyquist semicircles were fitted against electrical circuit, shown in Fig. 10. This circuit consist of solution resistance (R_S), a double layer capacitance (C_{dl}) and a charge transfer resistance (R_{ct}). The obtained data are shown in Table 6. The obtained Nyquist plots have depressed semi-circles with a single loop, suggesting single time constant participation in the EIS spectra[50]. The depression in semi-circle is because of inhomogeneity of electrode surface. The rise in diameter of capacitive loops with an increment in carbohydrazide Schiff base inhibitor concentration suggests an increase in the charge transfer resistance as a result of inhibitor adsorption on MS surface. The impedance efficiency was obtained by utilizing the accompanying equation:

$$\%I.E_{NY} = \frac{R_{ct}^{(inhi)} - R_{ct}^{(acid)}}{R_{ct}^{inhi}} * 100 \tag{9}$$

where, $R_{ct}^{(inhi)}$ and $R_{ct}^{(acid)}$ are the polarization resistance data in the inclusion along with exclusion of an inhibitor individually.

As the inhibitor concentration increases, C_{dl} reduces and R_{ct} increases as represented in Table 6, the results confirmed the high degree of adsorption of carbohydrazide Schiff base at MS/HCl interface by sharing of non-bonding heteroatoms electrons of inhibitor molecules to the vacant d-orbital of Fe. MBTC shows maximum 96.75% inhibition efficiency at 150 ppm against 320.67 Ωcm² R_{ct} value, Whereas CBTC shows maximum 95.14%
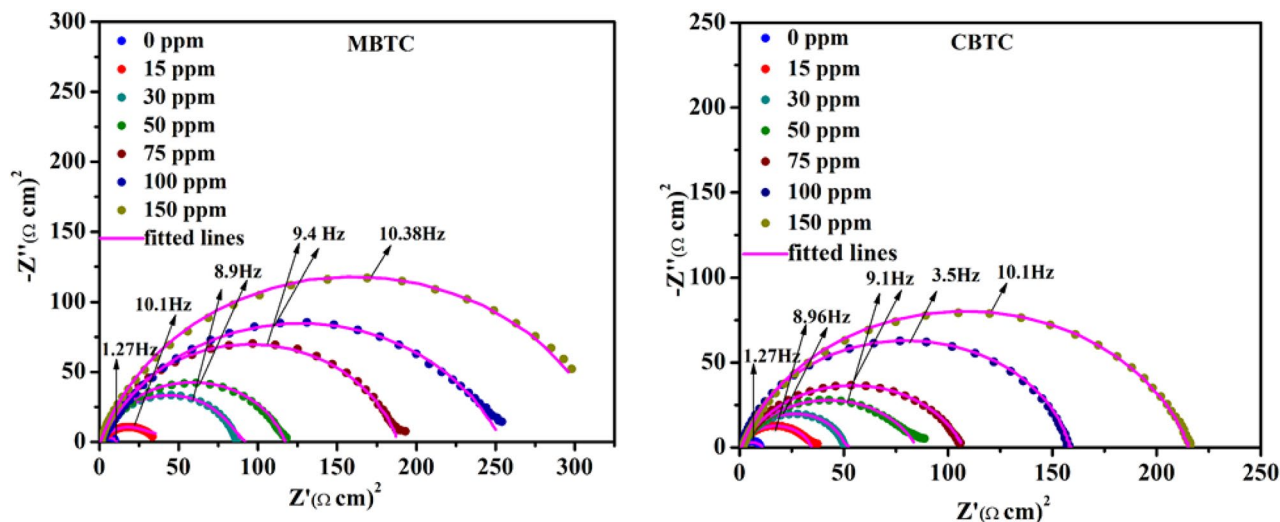
9

Figure 8. Nyquist plots for MBTC and CBTC carbohydrazide Schiff base inhibitors.
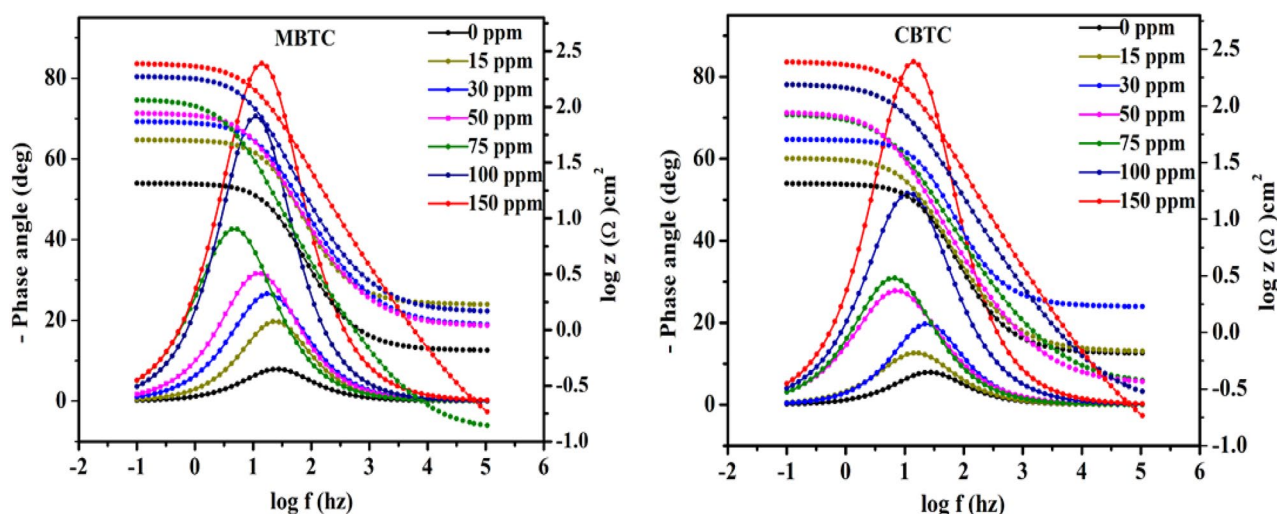

Figure 9. Bode plot for MBTC and CBTCcarbohydrazide Schiff base inhibitors.

against 214.48 Ω cm^2 R_{ct} value with R_{ct} value. It confirms that MBTC has better inhibition performance against the 15% HCl corrosive medium. The value of C_{dl} was obtained by equation

$$C_{dl} = \left(Y_0 R_{ct}^{inhi)1-n}\right)^{1/n} \tag{10}$$

where (Y_0) for proportional factor and (n) for phase shift and it is measured for the surface inhomogeneity.

In Bode plots continuing increment in the phase angle with concentration up to 150 ppm is related to the development of surface coverage by the inhibitors MBTC and CBTC molecules. The maximum height in the phase angle towards − 90°, the existence of single maxima demonstrates presence of one time constant related to electrical double layer at the surface solution interface[52].

The inhibition efficiency calculated by gravimetric, PDP, & EIS methods for MS in presence and absence of inhibitors in 15% HCl solution are in good agreement to each other. The high corrosion inhibition proficiency value of both studied MBTC and CBTC even at lower concentration suggested that MBTC and CBTC are good corrosion inhibitors for MS in acidic solution.

Surface morphology study.   *FESEM analysis.*   The surface morphology of polished MS, after 6 h of immersion in 15%HCl solution in the absence and presence of 150 ppm for MBTC and CBTC inhibitors are depicted in Fig. 11. From Fig. 11B, it is observed that the metallic surface is extremely corroded in HCl solution without inhibitor whereas polished sample (Fig. 11A) is smooth due to minor corrosion. However, Fig. 11C and D containing inhibitors show very smooth MS surface and it contain less cracks and pits due to adsorption of MBTC and CBTC inhibitors, respectively, at MS surface. Consequently, these inhibitors demonstrated that MS is protected against corrosion by forming protective layer of inhibitor at the surface of mild steel[53].

Figure 10. Equivalent circuit used for fitting EIS graphs.

Conc. (ppm)	R_S (Ω cm^2)	R_{ct} (Ω cm^2)	Y_0 (μF cm^{-2})	n	C_{dl} (μF cm^2)	IE$_{NY}$%
0	0.6561 ($\pm$0.012)	10.42 ($\pm$0.300)	764 ($\pm$0.573)	0.8744 ($\pm$0.001)	381.58 ($\pm$0.504)	–
MBTC						
15	0.8432 ($\pm$0.022)	37.22 ($\pm$0.551)	246.88 ($\pm$0.349)	0.8605 ($\pm$0.002)	115.42 ($\pm$0.442)	72.00 ($\pm$0.567)
30	0.8809 ($\pm$0.017)	62.89 ($\pm$0.315)	238.73 ($\pm$0.441)	0.8333 ($\pm$0.002)	103.10 ($\pm$0.365)	83.43 ($\pm$0.342)
50	0.8870 ($\pm$0.002)	105.18 ($\pm$0.203)	223.43 ($\pm$0.344)	0.8169 ($\pm$0.003)	96.39 ($\pm$0.278)	90.09 ($\pm$0.144)
75	0.4516 ($\pm$0.003)	187.00 ($\pm$1.09)	172.74 ($\pm$0.865)	0.8167 ($\pm$0.001)	79.94 ($\pm$0.675)	94.42 ($\pm$0.732)
100	0.6890 ($\pm$0.019)	256.00 ($\pm$0.675)	140.75 ($\pm$0.752)	0.8097 ($\pm$0.002)	64.45 ($\pm$0.867)	95.92 ($\pm$0.629)
150	0.6246 ($\pm$0.012)	320.67 ($\pm$1.331)	131.06 ($\pm$1.291)	0.8032 ($\pm$0.002)	60.28 ($\pm$0.652)	96.75 ($\pm$0.530)
CBTC						
15	0.6785 ($\pm$0.011)	33.82 ($\pm$0.211)	704.56 ($\pm$1.191)	0.8579 ($\pm$0.001)	379.40 ($\pm$0.761)	69.18 ($\pm$0.134)
30	0.6918 ($\pm$0.014)	48.80 ($\pm$0.453)	690.71 ($\pm$0.672)	0.8415 ($\pm$0.003)	364.74 ($\pm$0.870)	78.64 ($\pm$0.771)
50	0.3516 ($\pm$0.010)	84.67 ($\pm$1.213)	312.86 ($\pm$0.342)	0.8288 ($\pm$0.004)	276.91 ($\pm$0.528)	87.69 ($\pm$0.349)
75	0.8840 ($\pm$0.025)	137.89 ($\pm$0.567)	288.57 ($\pm$0.202)	0.8189 ($\pm$0.002)	141.42 ($\pm$0.923)	92.44 ($\pm$0.166)
100	0.6870 ($\pm$0.002)	157.09 ($\pm$0.214)	264.47 ($\pm$1.012)	0.8176 ($\pm$0.001)	130.07 ($\pm$0.591)	93.36 ($\pm$0.459)
150	0.8970 ($\pm$0.035)	214.48 ($\pm$1.092)	189.14 ($\pm$0.623)	0.8070 ($\pm$0.003)	87.98 ($\pm$0.491)	95.14 ($\pm$0.152)

Table 6. EIS data for carbohydrazideschiff base inhibitors.
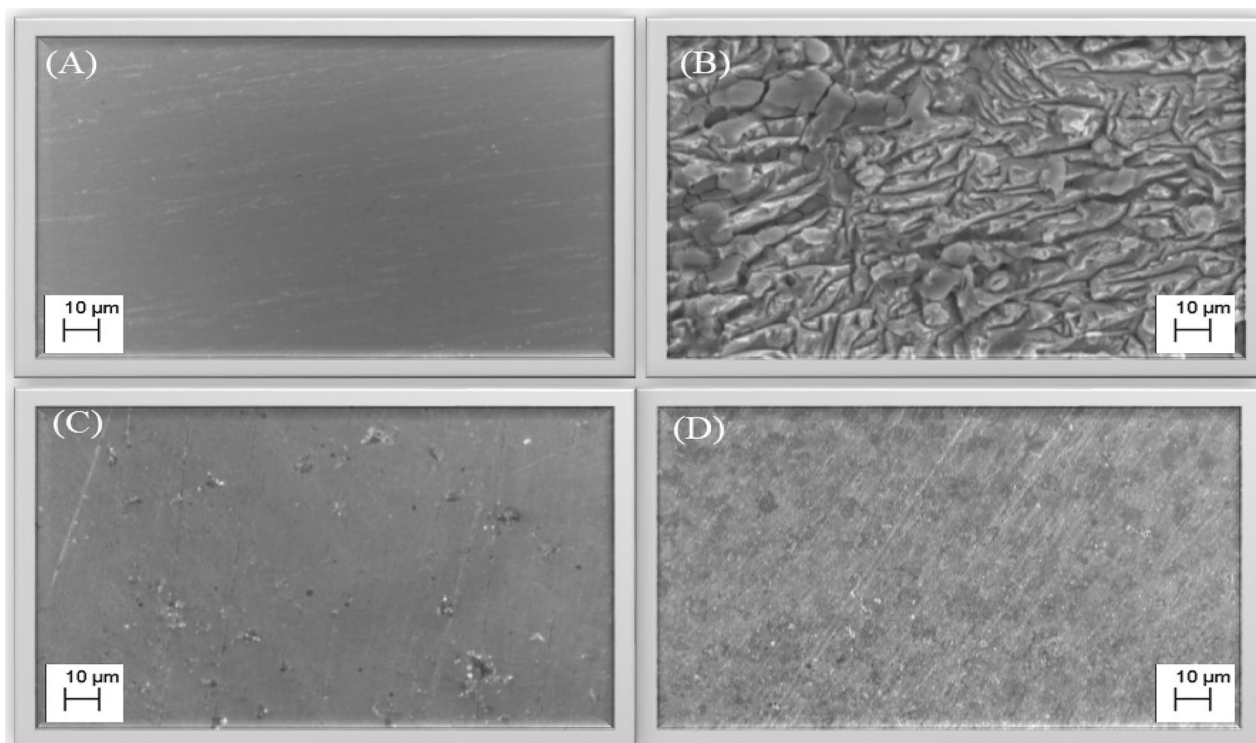

Figure 11. FESEM pictures of polished, blank, MBTC and CBTC inhibitor treated surface (**A–D**) respectively.
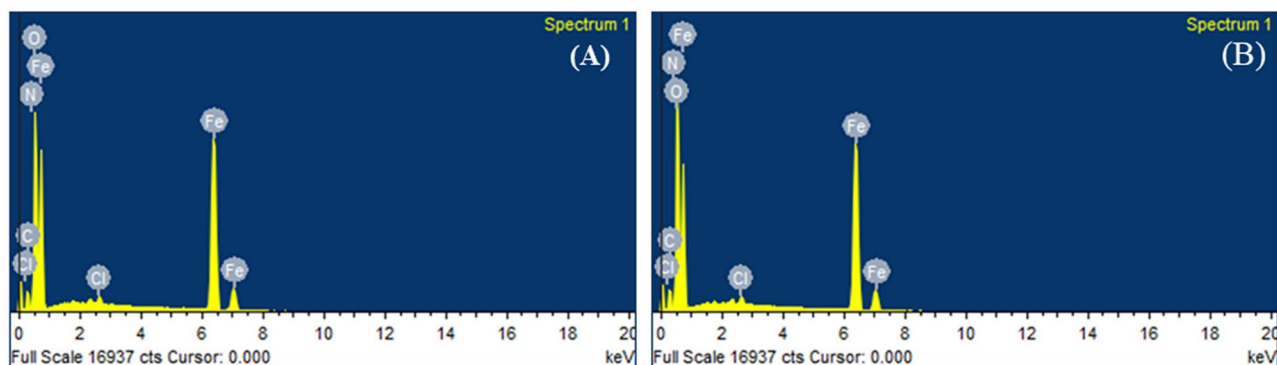
Figure 12. EDX spectra for (**A**) with MBTC (**B**) with CBTC inhibitors.

EDX analysis. The EDX images of MS surface containing MBTC and CBTC are shown in Fig. 12A,B, respectively. The presence of C, N, O, and Cl, confirms the presence of adsorbed inhibitor layer on MS surface[54].

AFM analysis. AFM analysis is an important technique for 3-D representation of surface with appropriate height profile of inhibitors. It consists of the important parameter of average roughness (R_{max}), average of maximum height (R_a), and the greatest separation among the maximum point and minimum points on the profile roughness (R_q). The AFM of samples are shown in Fig. 13. The result for the height profile for polished surface (Fig. 13A) are $R_{max} = 57.3$ nm, $R_q = 6.07$ nm, $R_a = 4.92$ nm. For blank sample (Fig. 13B) $R_{max} = 567$ nm, $R_q = 77.9$ nm, $R_a = 62.6$ nm. From Fig. 13C the surface with MBTC containing $R_{max} = 107$ nm, $R_q = 10.3$ nm, $R_a = 8.14$ nm and Fig. 13D, in presence of CBTC, $R_{max} = 156$ nm, $R_q = 20.0$ nm, $R_a = 15.4$ nm. The lower value of roughness in presence of inhibitors is because of the adsorption of inhibitor molecules on the MS surface[55].

XPS analysis. XPS is used to know the composition of adsorbed inhibitor layer on MS surface. Result of XPS analysis of MBTC and CBTC inhibitor are shown in Figs. 14 and 15 respectively.
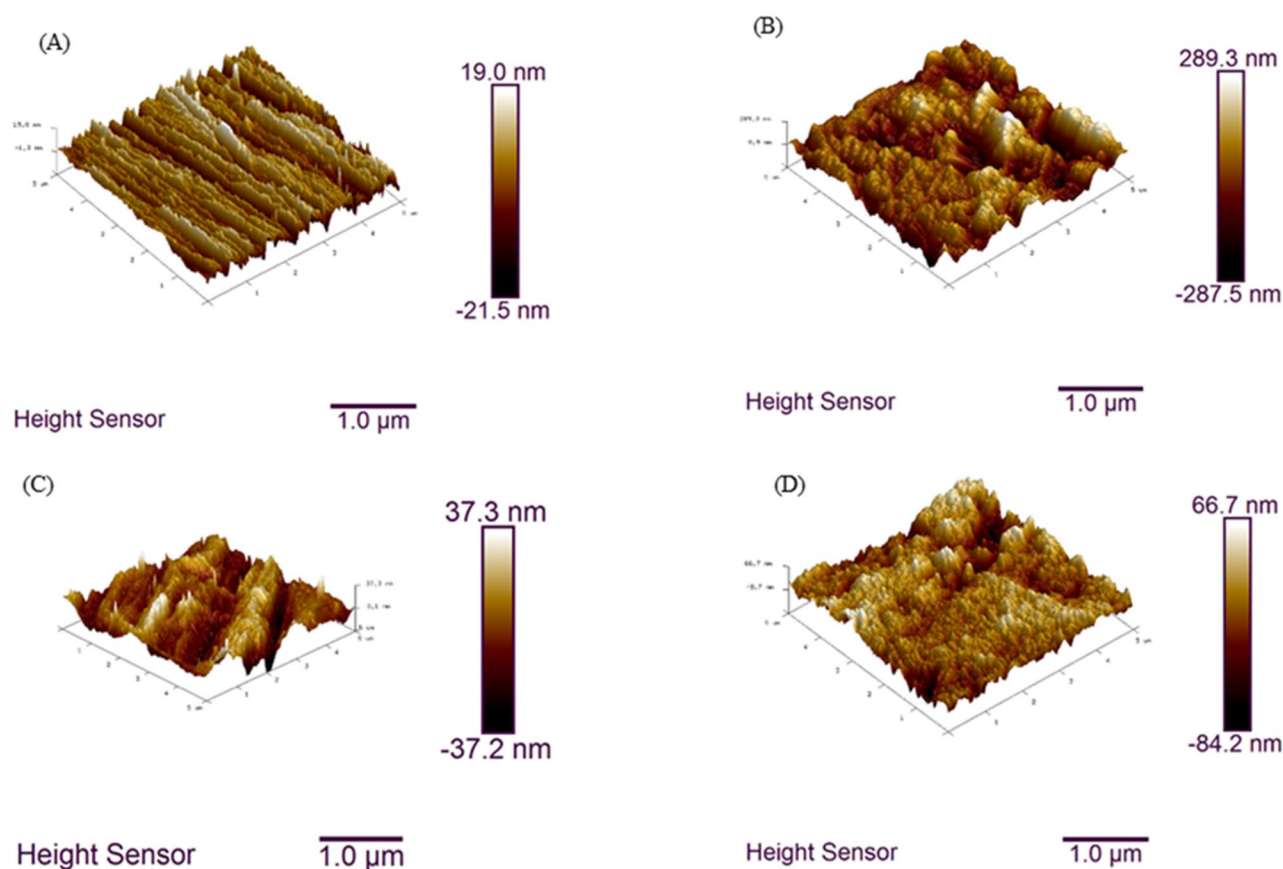
Figure 13. AFM images for polished (**A**), blank (**B**), with inhibitors MBTC (**C**), and CBTC (D).
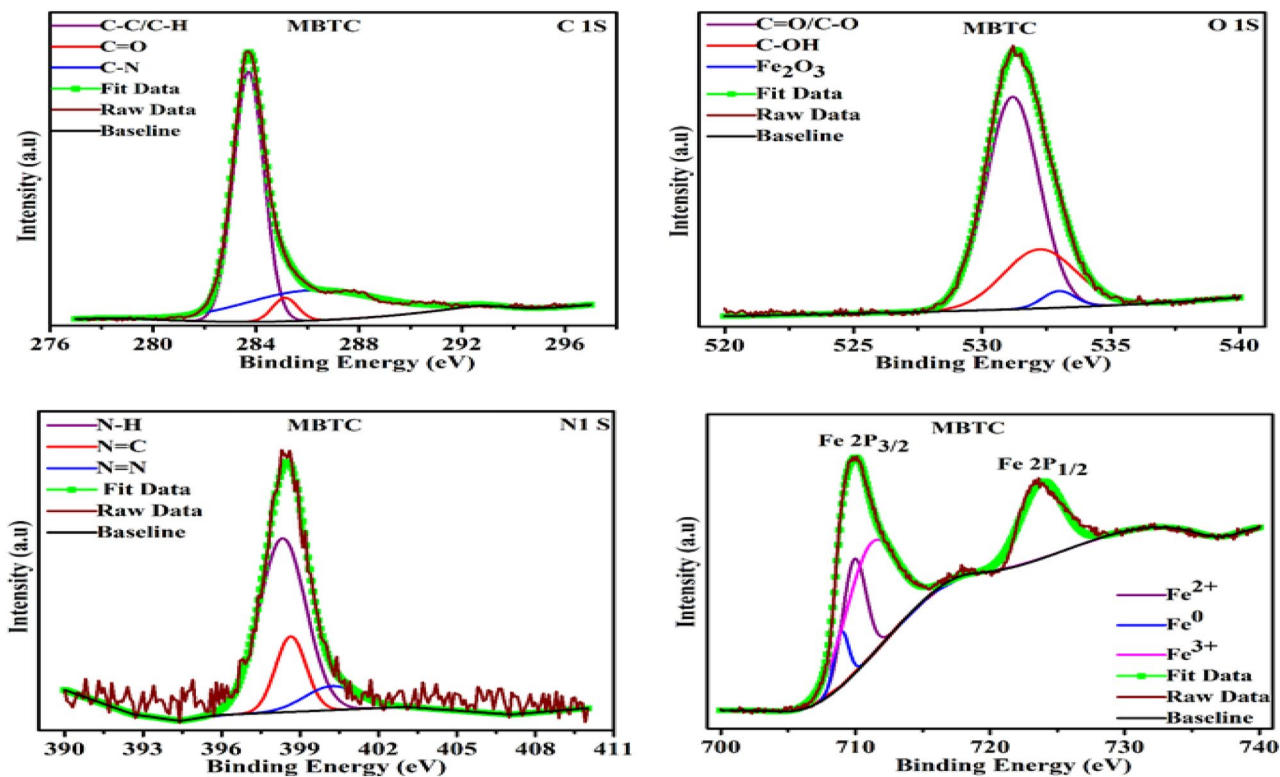
Figure 14. XPS spectra for deposited layer for MBTC inhibitors.
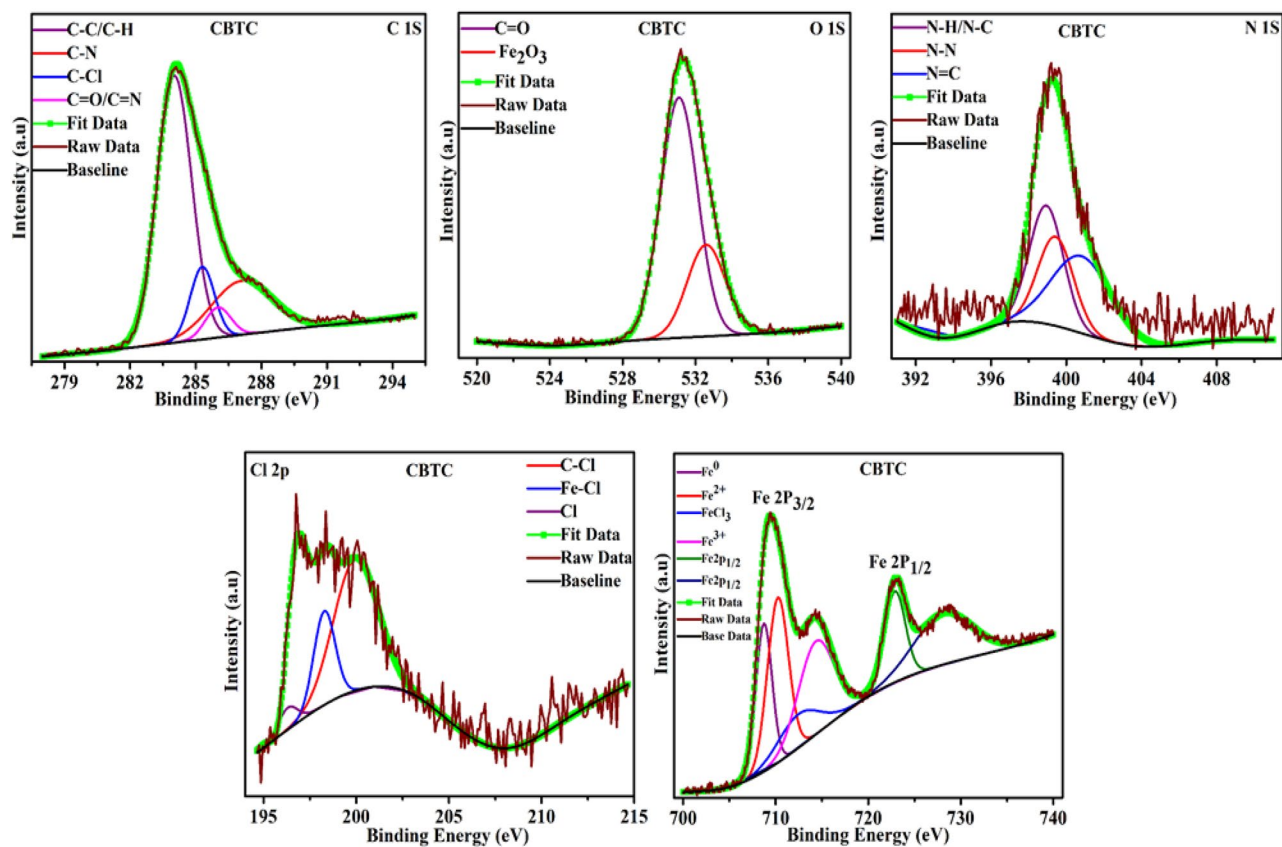

Figure 15. XPS spectra for deposited layer for CBTC inhibitors.

In Fig. 14, three peaks of C1s spectrum with binding energies of 283.76, 285.05, and 285.80 eV are assigned to the C–C or C–H, C=O and C–N bonds respectively[56,57]. The O1s peaks at 531.16 eV, 532.30 eV along with 533.09 eV, respectively, connected to O=C or C–O, C–OH, and Fe_2O_3[57,58]. Three peaks in the N1s spectrum, at 398.21, 398.76, and 400.30 eV are associated to N–H, N=C, and N=N, respectively[54,58]. The Fe $2P_{1/2}$ spectrum contains three peaks at 708.93, 710.20, 711.48 eV that are linked to metallic iron, Fe^{2+}, and Fe^{3+} whereas the spectrum Fe $2P_{3/2}$ only one peak at 723.72eV[33,58,59].

Four peaks of CBTC inhibitor adsorbed on the MS surface were observed in the C1s spectrum in Fig. 15. The peak at 284.07 eV corresponds to C–C or C-H aromatic bond. The peak for the C-atom in the C=O and C=N bonds are at 286.07 eV[59]. The C–Cl bond and the C–N bond at 285.29 and 287.03[54]. The peak for the Fe_2O_3 bond can be seen in the O1s spectrum at 532.77 eV, whereas the peak for C=O is at 531.19 eV[60]. The N1s spectrum represents three peaks at binding energy 398.74, 399.18, and 400.64 eV attributed for NH or NC bond, N–N bond and N=C bond of the inhibitor CBTC[3,61]. There are three peaks in the Cl 2P peak, with the peak at 196.41 eV for chlorine ion of the HCl solution, the peak at 198.21 eV representing the Fe-Cl bond, and the peak at 200.08 eV describing the C–Cl bond of the organic inhibitor[33,56]. The Fe 2P1/2 spectrum comprises four peaks for metallic iron, Fe^{2+}, $FeCl_3$, and Fe^{3+} at 708.70, 710.36, 713.28, and 714.56 eV, but Fe 2P3/2 has two peaks at 723.05 and 728.75 eV[62,63].

Theoretical analysis. *DFT results.* The optimized structures, HOMO/LUMO frontier orbitals as well as the molecular electrostatic potential (ESP) are represented in Fig. 16. Table 7 represents the main orbital parameters calculated for the MBTC and CBTC inhibitors.

The least amount of energy needed to excite an electron in a molecule is known as the energy gap ($\Delta E = E_{HOMO} - E_{LUMO}$). The complex produced on the metallic surface is very stable if the value of ΔE is low, indicating that the molecule's inhibitory effectiveness is strong. Hence, decreasing the value of ΔE enhances the molecule's reactivity, which makes adsorption easier and boosts the inhibitor's effectiveness[64]. In this work, the difference between the energy levels ΔE of MBTC (2.948 eV) and CBTC (2.951 eV) shows that MBTC has better corrosion-inhibiting properties than CBTC. Often the dipole moment (μ) because of the polarity of an inhibitor
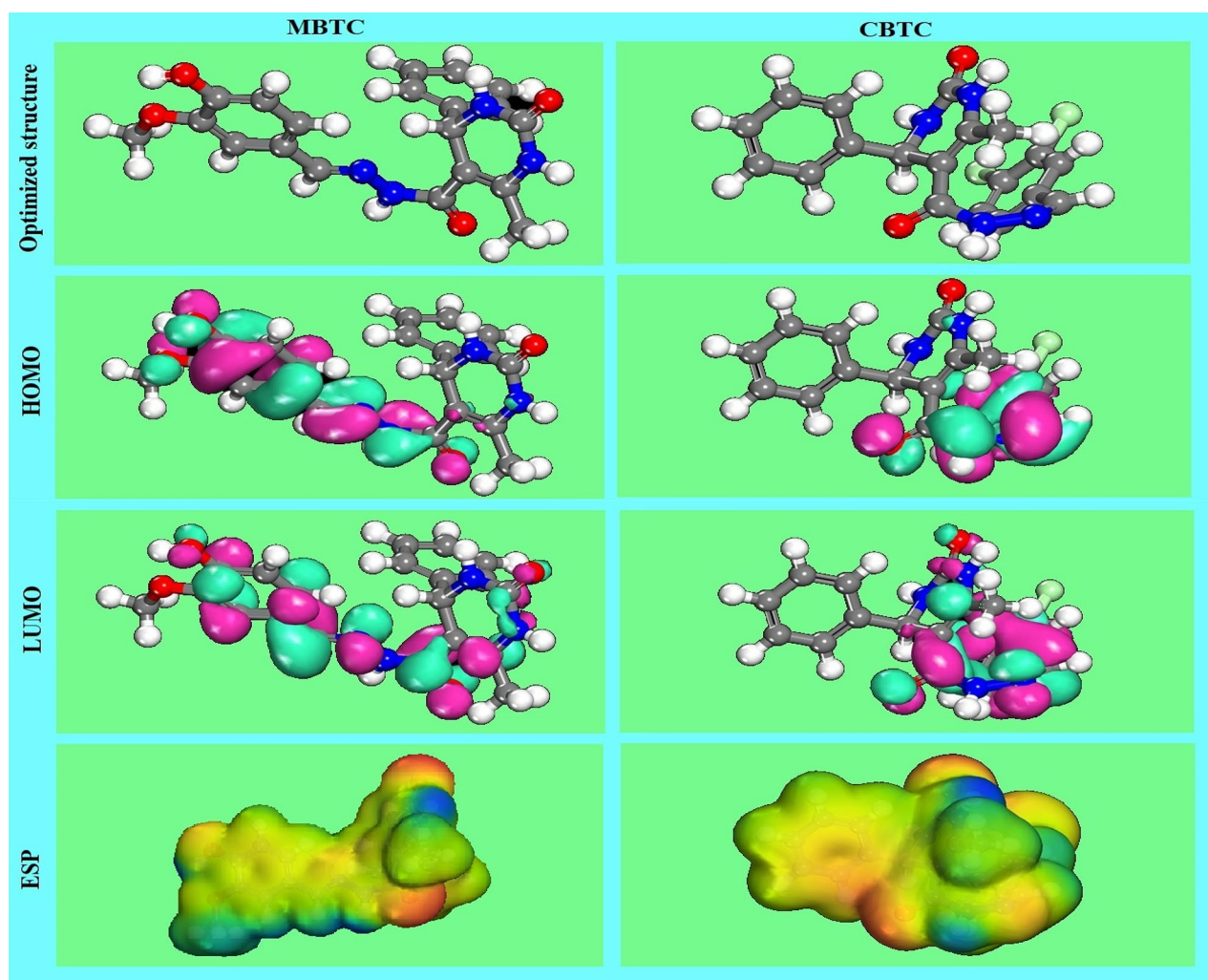

Figure 16. Molecular images of the MBTC and CBTC with optimized structures in HOMO, LUMO, and ESP.

Theoretical parameters	MBTC	CBTC
E_{HOMO} (eV)	− 5.134	− 5.656
E_{LUMO} (eV)	− 2.186	− 2.705
ΔE ($E_{HOMO} - E_{LUMO}$) (eV)	2.948	2.951
I (eV)	5.134	5.656
A (eV)	2.186	2.705
χ (eV)	3.660	4.180
η (eV)	1.474	1.475
σ (eV^{-1})	0.678	0.677
ΔN	1.132	0.955
$\Delta E_{back-donation}$	− 0.368	− 0.368
Dipole magnitude	9.562	4.126

Table 7. Calculated theoretical parameters for MBTC and CBTC molecules.

and is associated with the inhibitory capacity[65]. A high value of the μ results in significant inhibitory efficacy and increases the interaction (adsorption) of inhibitor compounds with a metal surface[42].Table 7 shows that the μ of the MBTC (9.562 Debye) is greater than μ of the CBTC (4.126 Debye). As well as, both inhibitors are greater than that of the H_2O molecule (1.88 Debye), which explains the significant inhibitory efficacy of the MBTC inhibitor. According to Table 7, the data of ΔN for both inhibitor is positive and greater than 3.6 (N > 3.6), which shows that electrons are transferred from both inhibitors studied to iron, promoting the development of coordination bond and thereby helping the formation of an adsorbed layer against corrosion.

To determine the active sites accountable for nucleophilic and electrophilic attacks, decided to use ESP surfaces as a useful descriptor. Figure 16 shows the ESP of the MBTC and CBTC molecules inhibitors study, the blue color shows the positive zones with nucleophilic reactivity, whereas yellow and red colors represent the negative zones with electrophilic reactivity.

As displayed in Fig. 16, the two inhibitors studied have 4 oxygen atoms possible electrophilic attack sites for the MBTC molecule and 2 possible electrophilic attack sites for the CBTC molecule. On the other hand, the two aromatic rings for the two compounds studied have a negative region. There are also on the two molecular structures of our inhibitors the 4 nitrogen atoms which are 4 other possible sites for the electrophilic attack. From the calculated zones of ESP, we notice that the potential negative zones possible are located on the electronegative atoms (N and O) and the unsaturated double bonds along with potential positive zones possible were located around the hydrogen atoms.

MC and MD simulations. The study of the adsorption behavior of the MBTC and CBTC molecules were examined on the surface of MS using MC and MD simulations[66–68].

Figure 17shows the adsorption equilibrium configurations for the two MBTC and CBTC molecules on the Fe (110) surface, thus two inhibitory molecules are adsorbed on the Fe (110) surface in almost parallel mode position (almost horizontal), indicating that the adsorbed inhibitor molecules cover the Fe surface well by developing a horizontal protective layer on the steel surface, which confirms the strong interactions among the heteroatoms (O, N) and the conjugated system of these inhibitors and atoms of iron.

Figure 18 displays the adsorption energy (E_{ads}) that was calculated by MC simulations of the MBTC and CBTC molecules with the surface of Fe (110). The compounds investigated are listed in the following order according to their effectiveness at inhibiting growth: MBTC > CBTC.

The most energetic stable positions of inhibitors are found by studying the temperature variations in MD simulation analyses. The little temperature drift in Fig. 19 indicates that the MD of our system was successful[69,70].

The bond length among the iron and the atoms of the MBTC and CBTC was determined by utilizing the radial distribution function (RDF) analysis of the MD trajectory in Fig. 20.Through estimating bond length data, different types of bonds formed was determined[39,71].The type of adsorption activity occurring on the metal is shown as peaks in the RDF plot at specific locations relative to the metal surface[41,72,73].The mechanism of chemisorption is reflected, when the peak is present between 1 and 3.5, but the RDF peaks are expected for physisorption at distances larger than 3.5[74–76].

The inhibition mechanism. The hypothesized corrosion mechanism of MBTC for MS in 15% HCl solutionis presented in Fig. 21, as determined by the experimental and theoretical investigations. Inhibitor molecules, by virtue of their adsorptive affinity, reject the pre-adsorbed H_2O molecules and corrosive species, finally adsorb on the surface of MS, therefore sheltering cathodic along with the anodic site[77,78]. This protects the surface against corrosion. In particular, because the compound possesses both a heterocyclic ring and other heteroatoms, as shown by the Mulliken charges, there is an increased predisposition toward surface adsorption[79]. These heteroatoms (O, N) and the conjugated system are able to donate lone pair electrons to the empty d-orbit of the iron atom[80].

Adsorption has an important role in corrosion prevention because the organic molecules are effectively and efficiently adsorbed on the surface, thus stop further deterioration on the surface of MS. All of the information
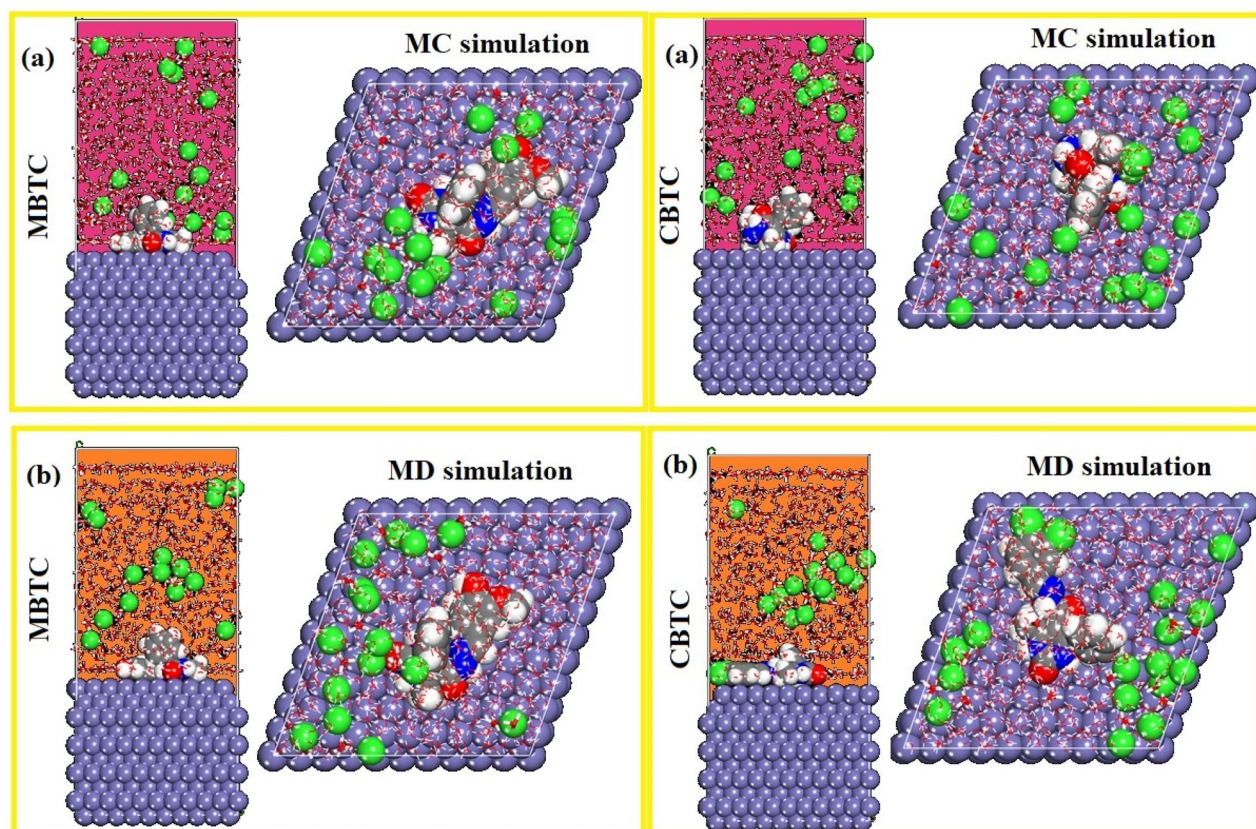
Figure 17. Results of MC (**a**) and MD (**b**) simulations: The equilibrium configurations of MBTC and CBTC molecules adhering to the surface of iron (110).
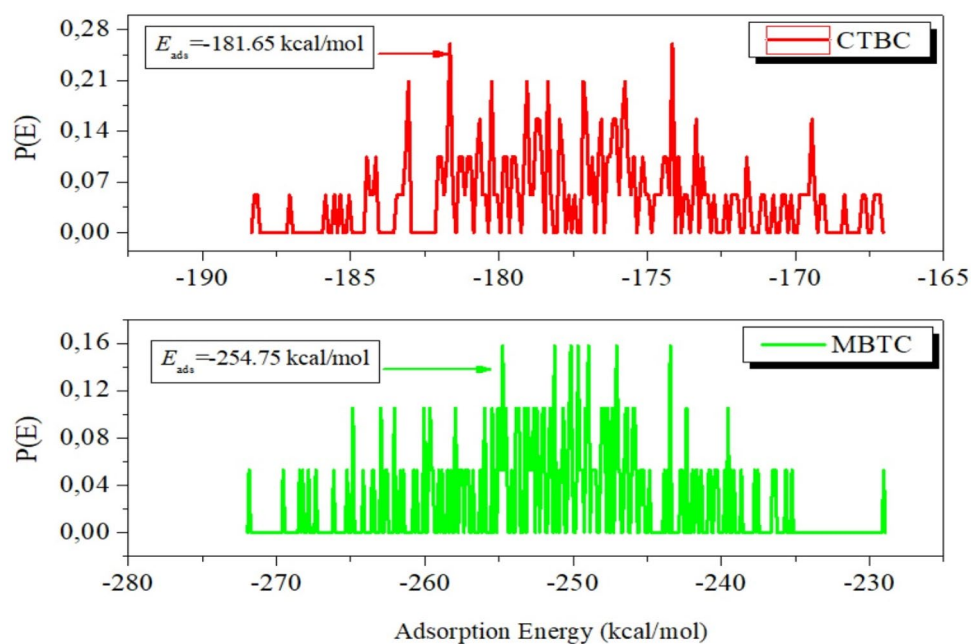

Figure 18. Distribution of the E_{ads} of MBTC and CBTC:MC simulations of the molecules on Fe (110) plane.
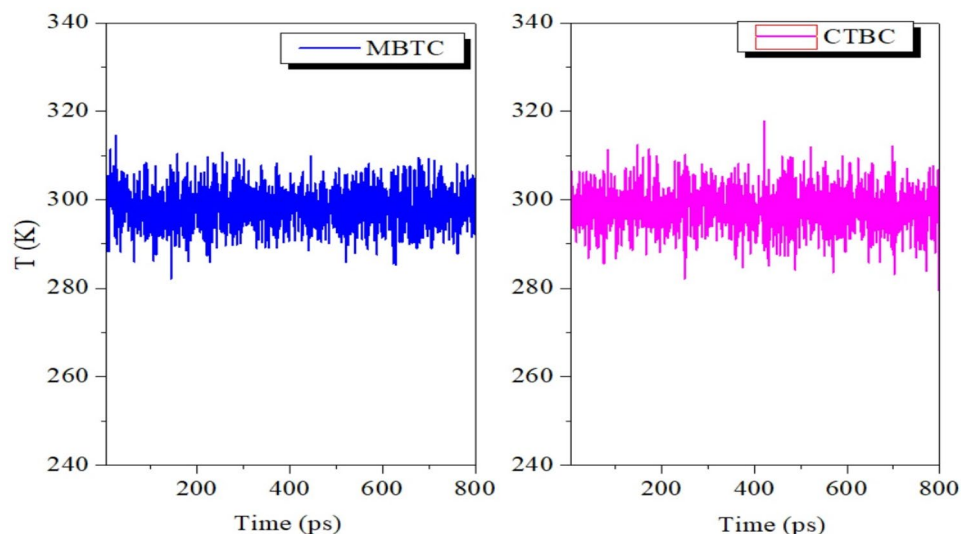
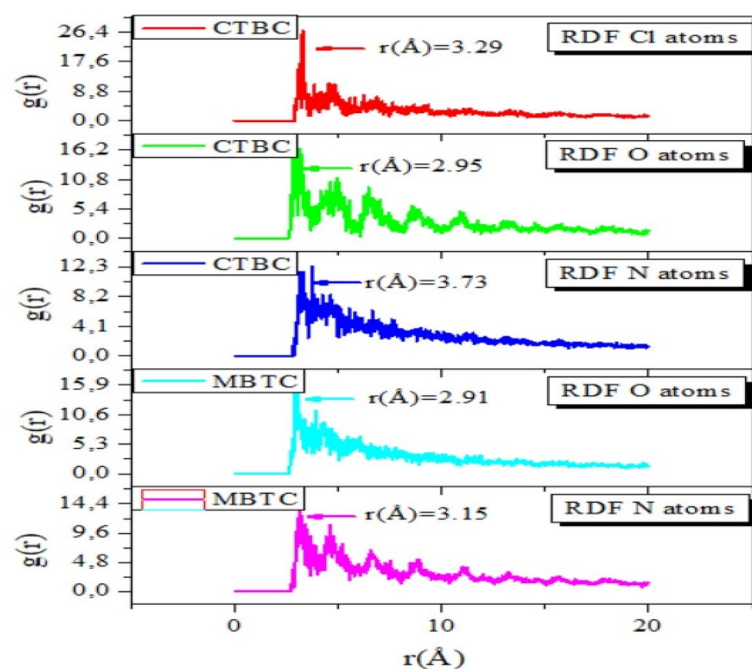**Figure 19.** Temperature fluctuation at 298 K during the MD run of MBTC and CBTC molecules on the Fe(110) plane.

Figure 20. RDF of O, N and Cl atoms of MBTC and CBTC in the simulated corrosion media on the Fe plane via MD.

mentioned in carbohydrazide Schiff bases supports this process. The thermodynamic properties of adsorption and theoretical calculations imply that the adsorption mechanism involves physical as well as chemical adsorption. Hence, carbohydrazide Schiff base adsorption on MS surface is explained by the donor–acceptor interactions, which link the electrons of nitrogen, oxygen, and the aromatic rings of inhibitors to the unoccupied d-orbitals of Fe surface atom. The ability of the inhibitor to specifically bind to the metal's surface and displace water molecules is responsible the corrosion-inhibiting process.

Conclusion
Both the studied Schiff base carbohydrazide compounds MBTC and CBTC contain pyrimidine as well as aromatic rings, heteroatoms (oxygen and nitrogen) and planar structures through which adsorb on the MS surface and act as efficient corrosion inhibitor. The inhibitors MBTC and CBTC offered efficiency of 97.45% and 95.89%,
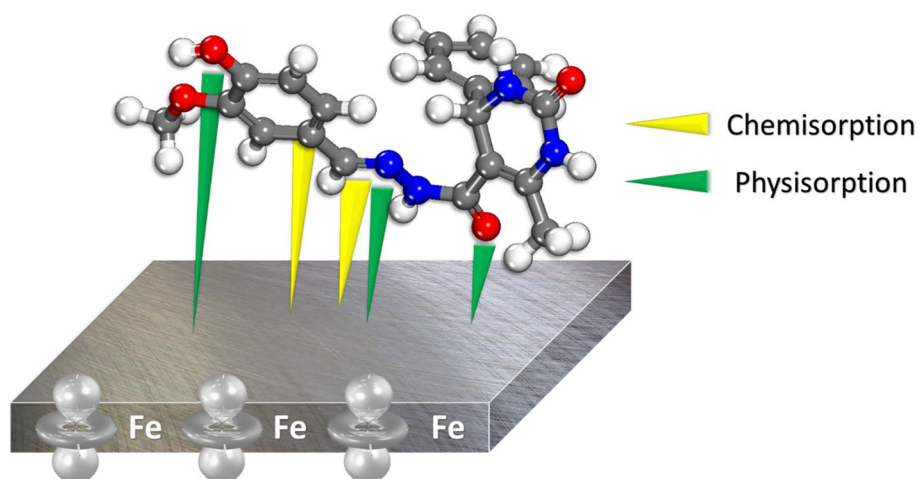
Figure 21. Diagram of the mechanisms of MBTC adsorption on mild steel.

respectively, at 150 ppm concentration. The efficiency offered by both inhibitors increased on increasing concentration and decreased on increasing temperature. The potentiodynamic polarization measurements concluded that MBTC and CBTC behave as mixed inhibitors. The inhibitors MBTC and CBTC adsorbed as per Langmuir isotherm and mixed adsorption process. The adsorption of inhibitors on MS surface was confirmed by the FESEM, EDX and XPS analysis. The analysis of the DFT-derived descriptors revealed that the molecules' heteroatoms are involved in the adsorption of these inhibitors onto the MS surface. As per MCS and MDS analysis, both inhibitors have a strong interaction, resulting in their adsorption onto the Fe (100) surface plane. This adsorption prevents corrosion activity from the MS surface.

Data availability
The authors declare that the data supporting the findings of this study are available within the paper.

References
1. El-Hamid, A. A. *et al.* Synthesis of gemini cationic surfactants-based pyridine Schiff base for steel corrosion and sulfate reducing bacteria mitigation. *J. Mol. Liq.* **369**, 120890 (2023).
2. Melhi, S. *et al.* Effective corrosion inhibition of mild steel in hydrochloric acid by newly synthesized Schiff base nano Co(II) and Cr(III) complexes: spectral, thermal, electrochemical and DFT (FMO, NBO) studies. *RSC Adv.* **12**, 32488 (2022).
3. Gupta, S. K., Mehta, R. K. & Yadav, M. Schiff bases as corrosion inhibitors on mild steel in acidic medium: Gravimetric, electrochemical, surface morphological and computational studies. *J. Mol. Liq.* **368**, 120747 (2022).
4. Nazir, U. *et al.* Corrosion inhibition studies of ferrocenyl Schiff bases in a mild acidic medium through experimental methods and DFT calculations. *New J. Chem.* **46**, 3925 (2022).
5. Salhi, A. *et al.* A correlated theoretical and electrochemical investigation of the corrosion inhibition performance of phenolic Schiff bases on mild steel in HCl solution (Part B). *Inorg. Chem. Commun.* **152**, 110684 (2023).
6. Messali, M. *et al.* A new schiff base derivative as an effective corrosion inhibitor for mild steel in acidic media: Experimental and computer simulations studies. *J. Mol. Struct.* **1168**, 39–48 (2018).
7. Fouda, A. S. & Abdallah, Y. M. Corrosion inhibition of aluminum-silicon alloy in 1 M HCl solution using phenazone and aminophenazone. *Arab. J. Sci. Eng.* **39**, 5363–5371 (2014).
8. AbdEl-Lateef, H. M., Shalabi, K. A., Arab, M. & Abdallah, Y. M. Corrosion mitigation performance of N80 steel in 5% sulfamic acid medium by applying novel tetrahydro-1,2,4-triazines including triazene moieties: Electrochemical and theoretical approaches. *ACS Omega* **7**, 23380–23392 (2022).
9. Abdallah, Y. M., Shalabi, K. & Bayoumy, N. M. Eco-friendly synthesis, biological activity and evaluation of some new pyridopyrimidinone derivatives as corrosion inhibitors for API 5L X52 carbon steel in 5% sulfamic acid medium. *J. Mol. Struct.* **1171**, 658–671 (2018).
10. Abdallah, Y. M. Electrochemical studies of phenyl sulphonylethanone derivatives compounds on corrosion of aluminum in 0.5 M H_2SO_4 solutions. *J. Mol. Liq.* **219**, 709–719 (2016).
11. Abdallah, Y. M., El-Gammal, O. A., Abd El-Lateef, H. & Shalabi, M. K. Synthesis and characterization of novel dicarbohydrazide derivatives with electrochemical and theoretical approaches as potential corrosion inhibitors for N80 steel in a 3.5% NaCl solution. *RSC Adv.* **12**, 14665 (2022).
12. Yassin, A. Y., Abdelghany, A. M., Shaban, M. M. & Abdallah, Y. M. Synthesis, characterization and electrochemical behavior for API 5L X70 carbon steel in 5% sulfamic acid medium using PVVH/PEMA blend filled with gold nanoparticles. *Colloids Surf. A* **635**, 128115 (2022).
13. El LateefH, M. A., Abu-Dief, A. M., Abdel-Rahman, L. H., Sanudo, E. C. & Aliaga-Alcalde, N. Electrochemical and theoretical quantum approaches on the inhibition of C1018 carbon steel corrosion in acidic medium containing chloride using some newly synthesized phenolic Schiff bases compounds. *J. Electroanal. Chem.* **743**, 120–133 (2015).
14. Saha, S. K., Dutta, A., Ghosh, P., Sukul, D. & Banerjee, P. Novel Schiff-base molecules as efficient corrosion inhibitors for mild steel surface in 1 M HCl medium: Experimental and theoretical approach. *Phys. Chem. Chem. Phys.* **18**, 17898 (2016).
15. Furtado, L. B. *et al.* Effects of temperature, concentration and synergism on green Schiff bases synthesized from vanillin in applications as corrosion inhibitors for carbon steel in well stimulation. *J. Petrol. Sci. Eng.* **213**, 110401 (2022).

16. Satpati, S., Suhasaria, A., Ghosal, S., Dey, S. & Sukul, D. Interaction of newly synthesized dipeptide Schiff bases with mild steel surface in aqueous HCl: Experimental and theoretical study on thermodynamics, adsorption and anti-corrosion characteristics. *Mater. Chem. Phys.* **296**, 127200 (2023).
17. Li, X. L. *et al.* 2-Pyridinecarboxaldehyde-based Schiff base as an effective corrosion inhibitor for mild steel in HCl medium: Experimental and computational studies. *J. Mol. Liq.* **345**, 117032 (2022).
18. Verma, C. & Quraishi, M. A. Recent progresses in Schiff bases as aqueous phase corrosion inhibitors: Design and applications. *Coord. Chem. Rev.* **446**, 214105 (2021).
19. Li, X. L. *et al.* Adsorption and corrosion inhibition performance of two planar rigid pyridinecarboxaldehyde-based double Schiff bases for mild steel in HCl solution: Experimental and computational investigations. *J. Mol. Liq.* **355**, 118926 (2022).
20. Satpati, S. *et al.* Anti-corrosive propensity of naturally occurring aldehydes and 1-(3-aminopropyl)imidazole condensed Schiff bases: Comparison on the effect of extended conjugation over electron donating substituents. *J. Mol. Struct.* **1268**, 133684 (2022).
21. Panda, A. K., Purohit, A. K., Upadhyay, A., Sahoo, M. K. & Kar, P. K. Corrosion inhibition studies on mild steel in HCl by a newly synthesized benzilmonohydrazone based Schiff base. *J. Indian Chem. Soc.* **98**, 100245 (2021).
22. Hamani, H., Daoud, D., Benabid, S. & Douadi, T. Electrochemical, density functional theory (DFT) and molecular dynamic (MD) simulations studies of synthesized three news Schiff bases as corrosion inhibitors on mild steel in the acidic environment. *J. Indian Chem. Soc.* **99**, 100492 (2022).
23. Fernandes, C. M. *et al.* Innovative characterization of original green vanillin-derived Schiff bases as corrosion inhibitors by a synergic approach based on electrochemistry, microstructure, and computational analyses. *Colloids Surf. A* **641**, 128540 (2022).
24. Amiery, A. A., Azzawi, W. K. & Isahak, W. N. R. W. Isatin Schif base is an effective corrosion inhibitor for mild steel in hydrochloric acid solution: Gravimetrical, electrochemical, and computational investigation. *Sci. Rep.* **12**, 17773 (2022).
25. Salhi, A. *et al.* Preventive behavior of phenol Schiff bases on mild steel corrosion in acidic medium part A: Experimental and molecular modeling approach. *Chem. Data Collect.* **39**, 100864 (2022).
26. Satpati, S., Saha, S. K., Suhasaria, A., Banerjee, P. & Sukul, D. Adsorption and anti-corrosion characteristics of vanillin Schiff bases on mild steel in 1 M HCl: experimental and theoretical study. *RSC Adv.* **10**, 9258 (2020).
27. Madani, A., Kaabi, I., Sibous, L. & Bentouhami, E. Synthesis, characterization and evaluation of the corrosion inhibition on mild steel of two new Schiff bases derived from 4, 4'-diaminobiphenyl: Density functional theory investigation. *J. Iran. Chem. Soc.* **18**, 3077–3095 (2021).
28. El Basiony, N. M., Elgendy, A., Nady, H., Migaheda, M. A. & Zaki, E. G. Adsorption characteristics and inhibition effect of two Schiff base compounds on corrosion of mild steel in 0.5 M HCl solution: Experimental, DFT studies, and Monte Carlo simulation. *RSC Adv.* **9**, 10473 (2019).
29. Behpour, M., Ghoreishi, S. M., Mohammadi, N., Soltani, N. & Salavati-Niasari, M. Investigation of some Schiff base compounds containing disulfide bond as HCl corrosion inhibitors for mild steel. *Corros. Sci.* **52**, 4046–4057 (2010).
30. Guo, W., Talha, M., Lin, Y. & Kong, X. Schiff's base with center of symmetry as an effective corrosion inhibitor for mild steel in acid medium: Electrochemical & simulation studies. *Colloids Surf. A* **615**, 126234 (2021).
31. Beena, K. P., Rajasekaran, A., Manna, P. K. & Suresh, R. Design, synthesis, characterization and biological evaluation of some substituted dihydropyrimidinone derivatives. *Der Pharm. Chem.* **8**(23), 57–62 (2016).
32. Yadav, M., Sinha, R. R., Kumar, S., Bahadur, I. & Ebenso, E. E. Synthesis and application of new acetohydrazide derivatives as a corrosion inhibition of mild steel in acidic medium: Insight from electrochemical and theoretical studies. *J. Mol. Liq.* **208**, 322–332 (2015).
33. Mehta, R. K., Gupta, S. K. & Yadav, M. Studies on pyrimidine derivative as green corrosion inhibitor in acidic environment: Electrochemical and computational approach. *J. Environ. Chem. Eng.* **10**, 108499 (2022).
34. Yadav, M., Gope, L., Kumari, N. & Yadav, P. Corrosion inhibition performance of pyranopyrazole derivatives for mild steel in HCl solution: Gravimetric, electrochemical and DFT. *Stud. J. Mol. Liq.* **216**, 78–86 (2016).
35. Dagdag, O. *et al.* Synthesis, physicochemical properties, theoretical and electrochemical studies of tetraglycidyl methylenedianiline. *J. Mol. Struct.* **1265**, 133508 (2022).
36. Daoudi, W. *et al.* Essential oil of Dysphania ambrosioides as a green corrosion inhibitor for mild steel in HCl solution. *J. Mol. Liq.* **363**, 119839 (2022).
37. Quadri, T. W. *et al.* Computational insights into quinoxaline-based corrosion inhibitors of steel in HCl: Quantum chemical analysis and QSPR-ANN studies. *Arab. J. Chem.* **15**, 103870 (2022).
38. Berdimurodov, E. *et al.* Novel gossypol–indole modification as a green corrosion inhibitor for low–carbon steel in aggressive alkaline–saline solution. *Colloids Surf. A* **637**, 128207 (2022).
39. Berdimurodov, E. *et al.* Novel glycoluril pharmaceutically active compound as a green corrosion inhibitor for the oil and gas industry. *J. Electroanal. Chem.* **907**, 116055 (2022).
40. Prasad, D. *et al.* Cinnamoum tamala leaves extract highly efficient corrosion bio-inhibitor for low carbon steel: Applying computational and experimental studies. *J. Mol. Liq.* **347**, 118218 (2021).
41. Dagdag, O. *et al.* Development and anti-corrosion performance of polymeric epoxy resin and their zinc phosphate composite on 15CDV6 steel in 3wt% NaCl: Experimental and computational studies. *J. Bio- Tribo-Corros.* **6**, 1–9 (2020).
42. Erramli, H. *et al.* Trifunctional epoxy resin as anticorrosive material for carbon steel in 1 M HCl: Experimental and computational studies. *Surf. Interfaces* **21**, 100707 (2020).
43. Dagdag, O. *et al.* Synthesis of macromolecular aromatic epoxy resins as anticorrosive materials: Computational modeling reinforced experimental studies. *ACS Omega* **5**, 3151–3164 (2020).
44. Dagdag, O. *et al.* Epoxy coating as effective anti-corrosive polymeric material for aluminum alloys: Formulation, electrochemical and computational approaches. *J. Mol. Liq.* **346**, 117886 (2020).
45. Kumari, N., Paul, P. K., Gope, L. & Yadav, M. Studies on anticorrosive action of synthesized indolines on mild steel in 15% HCl solution. *J. Adhes. Sci. Technol.* **31**, 1524–1544 (2016).
46. Yadav, M., Behera, D. & Kumar, S. Experimental and theoretical investigation on adsorption and corrosion inhibition properties of imidazopyridine derivatives on mild steel in hydrochloric acid solution. *Surf. Interface Anal.* **46**, 640–652 (2014).
47. Yadav, M., Behera, D., Kumar, S. & Yadav, P. Experimental and quantum chemical studies on corrosion inhibition performance of thiazolidinedione derivatives for mild steel in hydrochloric acid solution. *Chem. Eng. Commun.* **202**, 303–315 (2015).
48. Nazir, U., Akhter, Z., Ali, N. Z. & Shah, F. U. Experimental and theoretical insights into the corrosion inhibition activity of novel Schiff bases for aluminum alloy in acidic medium. *RSC Adv.* **9**, 36455 (2019).
49. Madani, A., Sibous, L., Hellal, A., Kaabi, I. & Bentouhami, E. Synthesis, density functional theory study, molecular dynamics simulation and anti-corrosion performance of two benzidine Schiff bases. *J. Mol. Struct.* **1235**, 130224 (2021).
50. Arsha, D. I. *et al.* Bis-Schiff bases of 2,20 -dibromobenzidine as efficient corrosion inhibitors for mild steel in acidic medium. *RSC Adv.* **10**, 4499 (2020).
51. Daoud, D., Hamani, H. & Douadi, T. Novel heterocyclic quinoline derivatives as green environmental corrosion inhibitors for carbon steel in HCl solution: experimental and theoretical investigation. *J. Adhes. Sci. Technol.* **35**, 2319–2345 (2021).
52. El Lateef, H. M. A., Abu-Dief, A. M. & Mohamed, A. A. Corrosion inhibition of carbon steel pipelines by some novel Schiff base compounds during acidizing treatment of oil wells studied by electrochemical and quantum chemical methods. *J. Mol. Struct.* **1130**, 522–542 (2017).

53. Sliem, M. H., El Basiony, N. M., Zaki, E. G., Sharaf, M. A. & Abdullah, A. M. Corrosion inhibition of mild steel in sulfuric acid by a newly synthesized Schiff base: An electrochemical, DFT, and Monte Carlo simulation study. *Electroanalysis* **32**, 3145–3158 (2020).

54. Mehta, R. K., Yadav, M. & Obot, I. B. Electrochemical and computational investigation of adsorption and corrosion inhibition behaviour of 2-aminobenzohydrazide derivatives at mild steel surface in 15% HCl. *Mater. Chem. Phys.* **290**, 126666 (2022).

55. Paul, P. K., Yadav, M. & Obot, I. B. Potential of dibenzo-18-crown-6-ether derivatives as a corrosion inhibitor on mild steel in HCl medium: Electrochemical and computational approaches. *New J. Chem.* **45**, 6826 (2021).

56. Paul, P. K., Yadav, M. & Obot, I. B. Investigation on corrosion protection behavior and adsorption of carbohydrazide-pyrazole compounds on mild steel in 15% HCl solution: Electrochemical and computational approach. *J. Mol. Liq.* **314**, 113513 (2020).

57. Paul, P. K., Mehta, R. K., Yadav, M. & Obot, I. B. Theoretical, electrochemical and computational inspection for anti-corrosion activity of triazepine derivatives on mild steel in HCl medium. *J. Mol. Liq.* **348**, 118075 (2022).

58. Yadav, M., Sarkar, T. K. & Obot, I. B. Carbohydrate compounds as green corrosion inhibitor: Electrochemical, XPS, DFT and molecular dynamics simulation studies. *RSC Adv.* **16**, 110053 (2016).

59. Saraswat, V., Kumari, R. & Yadav, M. Novel carbon dots as efficient green corrosion inhibitor for mild steel in HCl solution: Electrochemical, gravimetric and XPS studies. *J. Phys. Chem. Solids* **160**, 110341 (2022).

60. Sarkar, T. K., Saraswat, V., Mitra, R. K., Obot, I. B. & Yadav, M. Mitigation of corrosion in petroleum oil well/tubing steel using pyrimidines as efficient corrosion inhibitor: Experimental and theoretical investigation. *Mater. Today Commun.* **26**, 101862 (2021).

61. Gupta, S. K. *et al.* Diazenyl derivatives as efficient corrosion inhibitors for mild steel in HCl medium: Gravimetric, electrochemical and computational approach. *J. Mol. Liq.* **382**, 121976 (2023).

62. Sarkar, T. K., Yadav, M. & Obot, I. B. Mechanistic evaluation of adsorption and corrosion inhibition capabilities of novel indoline compounds for oil well/tubing steel in 15% HCl. *Chem. Eng. J.* **431**, 133481 (2022).

63. Paul, P. K. & Yadav, M. Investigation on corrosion inhibition and adsorption mechanism of triazine-thiourea derivatives at mild steel/HCl solution interface: Electrochemical, XPS, DFT and Monte Carlo simulation approach. *J. Electroanal. Chem.* **877**, 114599 (2020).

64. Ganjoo, R. *et al.* Experimental and theoretical study of sodium CocoylGlycinate as corrosion inhibitor for mild steel in hydrochloric acid medium. *J. Mol. Liq.* **364**, 119988 (2022).

65. Shaw, P., Obot, I. B. & Yadav, M. Functionalized 2-hydrazinobenzothiazolewith carbohydrates as a corrosion inhibitor: electrochemical, XPS, DFT and Monte Carlo simulation studies. *Mater. Chem. Front.* **3**, 931–940 (2019).

66. Tiwari, N., Mitra, R. K. & Yadav, M. Mitigation of corrosion in petroleum oil well/tubing steel using thiadiazolines as efficient corrosion inhibitor: Experimental and theoretical investigation. *Surf. Interfaces* **22**, 100770 (2021).

67. Bhardwaj, N. *et al.* Monte Carlo simulation, molecular dynamic simulation, quantum chemical calculation and anti-corrosive behaviour of Citrus limetta pulp waste extract for stainless steel (SS-410) in acidic medium. *Mater. Chem. Phys.* **284**, 126052 (2022).

68. Berdimurodov, E. *et al.* Novel gossypol–indole modification as a green corrosion inhibitor for low–carbon steel in aggressive alkaline–saline solution. *Colloids Surf. A* **637**, 128207 (2022).

69. El Faydy, M. *et al.* Insight into the corrosion inhibition of new bis-quinolin-8-ols derivatives as highly efficient inhibitors for C35E steel in 0.5 M H2SO4. *J. Mol. Liq.* **342**, 117333 (2021).

70. Molhi, A. *et al.* Performance of two epoxy resins against corrosion of C38 steel in 1M HCl: Electrochemical, thermodynamic and theoretical assessment. *Int. J. Corros. Scale Inhib.* **10**, 812–837 (2021).

71. Haldhar, R. *et al.* Anticorrosive properties of a green and sustainable inhibitor from leaves extract of Cannabis sativa plant: Experimental and theoretical approach. *Colloids Surf. A* **614**, 126211 (2021).

72. Bhardwaj, N., Sharma, P., Guo, L., Dagdag, O. & Kumar, V. Molecular dynamic simulation and Quantum chemical calculation of phytochemicals present in Beta vulgaris and electrochemical behaviour of Beta vulgaris peel extract as green corrosion inhibitor for stainless steel (SS-410) in acidic medium. *Colloids Surf. A* **632**, 127707 (2022).

73. Dagdag, O. *et al.* Cyclotriphosphazene based dendrimeric epoxy resin as an anti-corrosive material for copper in 3% NaCl: Experimental and computational demonstrations. *J. Mol. Liq.* **308**, 113020 (2020).

74. Molhi, A. *et al.* Contribution to the corrosion inhibition of C38 steel in 1 M hydrochloric acid medium by a new epoxy resin PGEPPP. *Int. J. Corros. Scale Inhib.* **10**, 399–418 (2021).

75. Berisha, A. Ab inito exploration of nanocars as potential corrosion inhibitors. *Comput. Theor. Chem.* **1201**, 113258 (2021).

76. Rahimi, A. *et al.* Novel sucrose derivative as a thermally stable inhibitor for mild steel corrosion in 15% HCl medium: An experimental and computational study. *Chem. Eng. J.* **446**, 136938 (2022).

77. Berisha, A., Podvorica, F. I. & Vataj, R. Corrosion inhibition study of mild steel in an aqueous hydrochloric acid solution using brilliant cresyl blue: A combined experimental and Monte Carlo study. *Port. Electrochim. Acta* **39**, 393–401 (2021).

78. El Arrouji, S. *et al.* Multidimensional analysis for corrosion inhibition by new pyrazoles on mild steel in acidic environment: Experimental and computational approach. *Chem. Data Collect.* **40**, 100885 (2022).

79. Jafari, H., Ameri, E., Rezaeivala, M. & Berisha, A. Experimental and theoretical studies on protecting steel against 0.5 M H$_2$SO$_4$ corrosion by new Schiff base. *J. Indian Chem. Soc.* **99**, 100665 (2022).

80. Mehmeti, V. Nystatin drug as an effective corrosion inhibitor for mild steel in acidic media: An experimental and theoretical study. *Corros. Sci. Technol.* **21**, 21–31 (2022).

Acknowledgements

Author contributions

S.K.G.: Inhibitor synthesis, formal analysis, writing—original draft. R.K.M.: Editing original draft and data analysis. M.Y.: Conceptualization, supervision, original draft review & editing. O.D.: DFT analysis. A.B.: MCS and MDS analysis. B.B.M.: MDS analysis. T.T.I.N.: MDS analysis. E.E.E.: Computational analysis and original draft review & editing. Shailendra Kumar Singh: Editing original draft and data analysis.

Competing interests

The authors declare no competing interests.

Additional information

Correspondence and requests for materials should be addressed to M.Y. or E.E.E.

Reprints and permissions information is available at www.nature.com/reprints.

Publisher's note Springer Nature remains neutral with regard to jurisdictional claims in published maps and institutional affiliations.